Optimal Bridge Retrofit Strategy to Enhance Disaster Resilience of Highway Transportation Systems

Morgan State University
The Pennsylvania State University
University of Maryland
University of Virginia
Virginia Polytechnic Institute & State University
West Virginia University

The Pennsylvania State University
The Thomas D. Larson Pennsylvania Transportation Institute
Transportation Research Building ❖ University Park, PA 16802-4710
Phone: 814-865-1891 ❖ Fax: 814-863-3707
www.mautc.psu.edu

Technical Report Documentation Page

1. Report No.	2. Government Accession No.	3. Recipient's Catalog No.
PSU-2012-01		

4. Title and Subtitle	5. Report Date
Optimal Bridge Retrofit Strategy to Enhance Disaster Resilience of Highway Transportation Systems	07/08/2014
	6. Performing Organization Code

7. Author(s)	8. Performing Organization Report No.
Swagata Banerjee, Sandhya Chandrasekaran and Ashok Venkittaraman	LTI 2014-11

9. Performing Organization Name and Address	10. Work Unit No. (TRAIS)
The Pennsylvania State University Larson Transportation Institute 201 Transportation Research Building University Park, PA 16802	11. Contract or Grant No. DTRT12-G-UTC03

12. Sponsoring Agency Name and Address	13. Type of Report and Period Covered
US Department of Transportation Research & Innovative Technology Admin UTC Program, RDT-30 1200 New Jersey Ave., SE Washington, DC 20590	Final 6/1/2012 – 12/31/2013
	14. Sponsoring Agency Code

15. Supplementary Notes

16. Abstract

This study evaluated the resilience of highway bridges under the multihazard scenario of earthquake in the presence of flood-induced scour. To mitigate losses incurred from bridge damage during extreme events, bridge retrofit strategies are selected such that the retrofit not only enhances bridge performance, but also improves resilience of the system consisting of these bridges. The first part of the report focuses on the enhancement of seismic resilience of bridges through retrofit. To obtain results specific to a bridge, a reinforced concrete bridge in the Los Angeles region was analyzed. This bridge was severely damaged during the Northridge earthquake due to shear failure of one bridge pier. A seismic vulnerability model of the bridge was developed through finite element analysis under a suite of time histories that represent regional seismic hazard. The obtained bridge vulnerability model was combined with appropriate loss and recovery models to calculate the seismic resilience of the bridge. The impact of retrofit on seismic resilience was observed by applying a suitable retrofit strategy to the bridge, assuming its undamaged condition prior to the Northridge event. A difference in resilience observed before and after bridge retrofit signified the effectiveness of seismic retrofit. The applied retrofit technique was also found to be cost effective through a cost-benefit analysis. A first-order, second-moment reliability analysis was performed and a tornado diagram developed to identify major uncertain input parameters to which seismic resilience is most sensitive. Statistical analysis of resilience obtained through random sampling of major uncertain input parameters revealed that the uncertain nature of seismic resilience can be characterized with a normal distribution, the standard deviation of which represents the uncertainty in seismic resilience. An optimal (with respect to cost and resilience) bridge retrofit strategy under multihazard was obtained in the second phase of this study. A multi-objective evolutionary algorithm, namely Non-dominated Sorting Genetic Algorithm II, was used. Application of this algorithm was demonstrated by retrofitting a bridge with column jackets and evaluating bridge resilience under the multihazard effect of earthquake and flood-induced scour. Three different retrofit materials—steel, carbon fiber, and glass fiber composites—were used. Required jacket thickness and cost of jacketing for each material differed to achieve the same level of resilience. Results from the optimization, called Pareto-optimal set, include solutions that are distinct from each other in terms of associated cost, contribution to resilience enhancement, and values of design parameters. This optimal set offers the best search results based on selected materials and design configurations for jackets.

17. Key Words	18. Distribution Statement
Optimization, resilience, seismic retrofit, flood-induced scour, fragility curves, cost-benefit	No restrictions. This document is available from the National Technical Information Service, Springfield, VA 22161

19. Security Classif. (of this report)	20. Security Classif. (of this page)	21. No. of Pages	22. Price
Unclassified	Unclassified	58	

DISCLAIMER

The contents of this report reflect the views of the authors, who are responsible for the facts and the accuracy of the information presented herein. This document is disseminated under the sponsorship of the U.S. Department of Transportation's University Transportation Centers Program, in the interest of information exchange. The U.S. Government assumes no liability for the contents or use thereof.

SUMMARY

This study was undertaken to evaluate the resilience of highway bridges under the multihazard scenario of earthquake in the presence of flood-induced scour. To mitigate losses incurred from bridge damage during extreme events, bridge retrofit strategies must be selected such that the retrofit not only enhances bridge performance but also improves the resilience of the system to which these bridges belong. The first part of the report focuses on the enhancement of the seismic resilience of bridges through retrofit. To obtain results specific to a bridge, a reinforced concrete bridge in the Los Angeles region was analyzed. This bridge was severely damaged during the Northridge earthquake due to shear failure of one bridge pier. A seismic vulnerability model of the bridge was developed through finite element analysis under a suite of time histories that represent a regional seismic hazard. The obtained bridge vulnerability model was then combined with appropriate loss and recovery models to calculate the seismic resilience of the bridge. The impact of retrofit on seismic resilience was observed by applying a suitable retrofit strategy to the bridge, assuming its undamaged condition prior to the Northridge event. The difference in resilience observed before and after bridge retrofit signified the effectiveness of the seismic retrofit. The applied retrofit technique was also found to be cost effective through a cost-benefit analysis. A first-order, second-moment reliability analysis was performed and a tornado diagram was developed to identify major uncertain input parameters to which seismic resilience is most sensitive. Statistical analysis of the resilience obtained through random sampling of major uncertain input parameters revealed that the uncertain nature of seismic resilience can be characterized by a normal distribution, the standard deviation of which represents the uncertainty in seismic resilience.

An optimal (with respect to cost and resilience) bridge retrofit strategy under a multihazard scenario was obtained in the second phase of this study. A multi-objective evolutionary algorithm, namely Non-dominated Sorting Genetic Algorithm II, was used. Application of this algorithm was

demonstrated by retrofitting a bridge with column jackets and evaluating bridge resilience under the multihazard effect of earthquake and flood-induced scour. Three different retrofit materials—steel, carbon fiber, and glass fiber composites—were used. The required jacket thickness and cost of jacketing for each material differed to achieve the same level of resilience. Results from the optimization, called Pareto-optimal set, include solutions that are distinct from each other in terms of associated cost, contribution to resilience enhancement, and values of design parameters. This optimal set offers the best search results based on selected materials and design configurations for jackets.

TABLE OF CONTENTS

1. INTRODUCTION 1

2. ENHANCING SEISMIC RESILIENCE THROUGH RETROFITTING 6

2.1 Seismic Resilience 6
2.2 Fragility Function 7
2.3 Loss and Recovery Functions 8
2.4 Testbed Bridge 10
2.5 Validation of Finite Element Model of the Bridge 12
2.6 Bridge Fragility Curves 14
2.7 Direct And Indirect Losses due to the Northridge Earthquake 17
2.8 Seismic Resilience 17
2.9 Bridge Seismic Retrofit and Enhancement in Resilience 18

3. SENSITIVITY ANALYSIS AND UNCERTAINTY ANALYSIS 21

3.1 Uncertain Parameters 21
3.2 Methods for Sensitivity Analysis 23
3.3 Uncertainty of Seismic Resilience 24

4. COST-BENEFIT ANALYSIS 27

4.1. Cost of Retrofit 27
4.2. Benefit from Retrofit 27
4.3. Benefit-Cost Ratio 29

5. RESILIENCE UNDER MULTIHAZARD SCENARIO 30

5.1. Multihazard Scenario for Bridges 30
5.1.1. Seismic Hazard……..... 30
5.1.2 .Flood Hazard..... 30
5.2. Identification of Optimal Bridge Retrofit Strategy for Multihazard……...32
5.2.1..Multi-Objective Optimization Program …….. 32
5.2.2 .Mechanical Properties of Selected Retrofit Material……... 35
5.2.3 Cost Objective……... 36
5.3. Model of a Case Study Bridge 36
5.4. Retrofit Design Domain 39
5.5. Optimal Retrofit Solution 42

6. CONCLUSIONS 45

REFERENCES 47

LIST OF FIGURES

Figure 2.1: Schematic Representation of Disaster Resilience and Post-Event Recovery Functions (a) Functionality Curve, (b) Linear Recovery Function, (c) Trigonometric Recovery Function and (d) Negative Exponential Recovery Function....7

Figure 2.2: (a) The Testbed Bridge (Schematic), (b) Cross-Section of Bridge Girder, and (c) Cross-Sections of Type 'H' and 'M' Piers the Testbed Bridge 10

Figure 2.3: Moment-Rotation Diagrams of Piers in Bent 5 to Bent 8 13

Figure 2.4: Seismic Fragility Curves of the Testbed Bridge at Four Damage States 17

Figure 2.5: Moment Rotation Diagrams of Retrofitted Piers in Bents 6, 7, and 8 19

Figure 2.6: Fragility Curves at Minor Damage State of the Retrofitted Bridge 20

Figure 3.1: Relative Variance of Uncertain Parameters 24

Figure 3.2: Tornado Diagram with Uncertain Parameters 24

Figure 3.3: Variation of Resilience with Recovery Time T_{RE} and Control Time T_{LC}....25

Figure 3.4: Uncertainty in Seismic Resilience of the Bridge Estimated for the Northridge Earthquake: (a) Normal Probability Paper and (b) Normal CDF 26

Figure 5.1: Regional Flood Hazard for Sacramento County in CA: (a) Historic Flood Data and (b) Flood Hazard Curve 31

Figure 5.2 Pareto-Optimal Set of Solutions....33

Figure 5.3: Flowchart of Multi-Objective Optimization for Retrofit Design of Bridges under Multihazard....35

Figure 5.4: (a) Schematic of the Case Study Bridge, (b) Girder Cross-Section, (c) Column Cross-Section and (d) Displacement-Based Fiber Element of Column Cross-Section In Opensees 38

Figure 5.5: Fragility Curves of the Bridge with 2.4 m Scour: (a) Original Bridge with No Retrofit, (b) Retrofitted Bridge with 12.7-mm-thick Steel Jacket, (c) Retrofitted Bridge with 2.54-mm-thick Carbon Fiber Jacket, and (d) Retrofitted Bridge with 2.54-mm-thick E-Glass Fiber Jacket....41

Figure 5.6: Resilience and Loss Ratios of the Case Study Bridge for Four Retrofit Cases....42

Figure 5.7: Pareto Fronts from (a) Generation 1, (b) Generation 2, and (c) Generation 3 43

LIST OF TABLES

Table 2.1: Mean and Standard Deviation of Post-Seismic Restoration Times For Highway Bridges 9

Table 2.2: Comparison of Modal Shapes and Fundamental Time Periods of the Bridge 14

Table 2.3: Shear Capacities and Shear Demand at Bridge Piers…… 14

Table 2.4: Drift Ratios and Threshold Values Rotation Ductility 16

Table 3.1: Fragility Parameters with 90% Confidence Intervals 23

Table 4.1: Summary of Benefit-Cost Ratio 29

Table 5.1: Calculation of Scour 39

Table 5.2a: Retrofit Design Solutions From Generation 1 44

Table 5.2b: Retrofit Design Solutions From Generation 2 44

Table 5.2c: Retrofit Design Solutions From Generation 3 44

1. INTRODUCTION

1.1 Problem Statement

A natural disaster is the consequence of an extreme natural hazard such as an earthquake, flood, hurricane, tornado, or landslide. It leads to economic, human and/or environmental losses to a society. The resulting loss depends on the ability of the affected population to survive the extreme event and recover from it, or in other words, the population's resilience. Disaster resilience is defined by the National Academics as "the ability to prepare and plan for, absorb, recover from, and more successfully adapt to adverse events" (Cutter et al. 2013). It has also been mentioned that "enhanced resilience allows better anticipation of disasters and better planning to reduce disaster losses—rather than waiting for an event to occur and paying for it afterward." To achieve such enhancement in resilience, it is important that the post-event recovery of the affected system or society be successfully performed within an acceptable level of time and cost.

Bridges are significant components of highway transportation systems that serve as a key mode of ground transportation and sometimes act as an important feeder system to other modes such as railroad systems, port facilities, and air travel. Bridge damage not only causes direct economic losses from required post-event bridge repair and restoration, but also produces indirect losses arising from network downtime, traffic delays, and business interruptions. The failure of large numbers of highway bridges in California during the 1971 San Fernando, 1989 Loma Prieta, and 1994 Northridge earthquakes severely disrupted the normal functionality of regional highway transportation systems and caused sudden and undesired changes in technical, organizational, societal, and economic conditions of the communities served by these systems. Prevention is better than a cure; this simple yet powerful adage becomes of profound importance in the event of a disaster. Along this line of thought, "recovery" and "resilience" have become key points in dealing with extreme events, if not in order to prevent them

completely, then to minimize their negative consequences by maximizing the disaster resilience of highway transportation systems. Retrofitting of highway bridges is one of the most common approaches undertaken by state Departments of Transportation (state DOTs) and by bridge owners to enhance system performance during extreme events.

Common seismic retrofit techniques for bridges include lateral confinement of bridge piers using steel or composite jackets, installation of restrainers at abutments and expansion joints, seismic isolation through bearings, and installation of bigger foundations (Caltrans 2011, WSDOT 2011, Wright et al. 2011). From decade-long research, it has been identified that confinement of bridge columns using wrap-around jackets has a positive impact on seismic resistance owing to enhanced shear and flexure capacity of bridge columns (Priestley et al. 1996, Haroun and Elsanadedy 2005). While bridge retrofit techniques may be effective in mitigating the seismic risk of bridges, the adequacy of their application and relative effectiveness greatly depend on the demand from seismic hazards specific to a bridge, enhancement in seismic functionality of highway transportation systems, and benefit-to-cost ratio for bridge retrofitting. In this context, the calculation of resilience is identified as a meaningful way to express loss and recovery of system functionality immediately after a natural disaster (Chang and Nojima 2001, Bruneau et al. 2003, Chang and Chamberlin 2004, Shinozuka et al. 2004, Rose and Liao 2005, Amdal and Swigart 2010, Cimellaro et al. 2010).

Besides single-hazard scenarios, bridges may be exposed to multiple-hazard or multihazard conditions during their service lives. There is a growing recognition of the need for multihazard disaster mitigation strategies for bridges among the global structural engineering community (Ghosn et al. 2003, MCEER-AEI 2007, Alampalli and Ettouney 2008). Effects of multiple hazards can enhance bridge vulnerability beyond that due to the effect of a single-hazard scenario, and thus may significantly reduce the disaster resilience of transportation infrastructure systems. Flood-induced soil erosion, commonly

known as scour, causes loss of lateral support at bridge foundations (Richardson and Davis 2001), and thus imposes additional flexibility that may amplify the effect of any other extreme natural hazard on bridge performance. Some researchers have also stated that the increased flexibility due to scour may even reduce the effect of an extreme natural hazard like an earthquake on bridge performance (Ghosn et al. 2003). Therefore, among several possible combinations of extreme hazards, an earthquake in the presence of flood-induced scour is a critical multi-hazard scenario for bridges located in seismically active, flood-prone regions.

Seismic vulnerability analysis of typical California bridges pre-exposed to foundation scour resulting from various intensity flood events revealed significant deterioration of the seismic performance and an increase in the seismic risk of these bridges, even under the effect of moderate scour (Banerjee and Prasad 2013). While multiple risk mitigation strategies can be simultaneously applied for multiple hazards, such a process may not always be feasible for various practical reasons, including bridge geometry, accessibility, and total cost available for hazard mitigation. Depending upon whether the mitigation operations are contradictory or complimentary with respect to the multiple hazards, there is scope to optimize the retrofit design in order to ensure overall structural reliability and the cost efficiency of retrofit.

The present study aims at optimizing the restoration costs associated with a bridge that has suffered multihazard damage under flood-induced scour and earthquake. The two conflicting objectives in the problem are maximizing bridge resilience and minimizing retrofit cost. Uneconomical retrofit design leads to mismanagement of funds allocated for restoration. There is, hence, a need for an effective tool to aid the design decision making process in order to achieve a high retrofit benefit against the resources expended. The past decade has seen the emergence of the application of evolutionary algorithms in the demonstration of structural design. A class of evolutionary algorithms namely Genetic

Algorithms (GAs) are a metaheuristic tool developed based on the biological theory of evolution to carry out search operations to arrive at the global extrema for a given objective function within its domain. Bocchini and Frangopol (2012) presented an optimization procedure that maximizes the resilience and minimizes restoration time for an entire bridge network under seismic damage. Fallah and Zamiri (2012) presented the optimal design of a base isolation system using a multi-objective genetic algorithm.

1.2 Orientation of the Report

The study first evaluated the effectiveness of retrofit techniques to enhance the seismic resilience of highway bridges. A reinforced concrete bridge in the La Cienega-Venice Boulevard sector of Santa Monica (I-10) freeway in Los Angeles, Calif., was selected as a testbed bridge. This freeway runs across eight states, from Florida to the Pacific. In 1993, this freeway was reported to be the world's busiest freeway, carrying an approximate average daily traffic (ADT) of 261,000 (U.S. Department of Transportation 2002). During the 1994 Northridge earthquake, this testbed bridge was severely damaged primarily due to shear failure of one of the bridge piers. Post-event reconnaissance indicated that the failure was initiated from inadequate lateral confinement of pre-1971 designed bridge piers. Due to this, the vertical load-carrying capacity of the bridge was reduced significantly during the seismic event, resulting in crushing of core concrete and buckling of longitudinal rebars of bridge piers (Cofer et al. 1997). Seismic vulnerability of the pre-damaged bridge was assessed through finite element (FE) analysis of the bridge under a suite of time histories that represent seismic hazard at the bridge site. Seismic resilience of the as-built bridge was calculated using appropriate loss and recovery models. To observe the effectiveness of bridge retrofit in enhancing seismic resilience, bridge piers were retrofitted with steel jackets, assuming the undamaged condition of the bridge prior to the Northridge event. Seismic vulnerability of the retrofitted bridge was estimated to calculate seismic resilience after

retrofitting. The difference in seismic resilience before and after retrofit is considered to be a signature representing the adequacy and effectiveness of the applied retrofit technique. A cost-benefit study was performed assuming a 30- to 50-year service life for the retrofitted bridge to evaluate the cost effectiveness of the applied seismic retrofit technique.

A first-order, second-moment (FOSM) reliability analysis was performed to identify major uncertain input parameters to which seismic resilience of the original un-retrofitted bridge estimated for the Northridge earthquake is most sensitive. For this, parameter uncertainties associated with bridge vulnerability analysis and resilience estimation modules were considered. A tornado diagram was developed to further support the observations made from FOSM analysis regarding the hierarchy of uncertain input parameters. To characterize the uncertain nature of seismic resilience, a statistical analysis of resilience was performed through random sampling of major uncertain input parameters.

The study was further extended to identify cost-effective risk mitigation strategies applied to, for example, the Caltrans bridge under multihazard (flood and earthquake) scenario. This was achieved through a multi-objective optimization technique, the objectives being cost and resilience. A multi-objective evolutionary algorithm, namely Non-dominated Sorting Genetic Algorithm II (NSGA II), was utilized owing to its implicit elitism and lower computational complexity (Deb 2001, Deb et al. 2002).

2. ENHANCING SEISMIC RESILIENCE THROUGH RETROFITTING

The seismic resilience of a highway bridge can be represented as an integrated measure of bridge seismic performance, expected losses, and recovery after the occurrence of seismic events. Therefore, calculation of bridge resilience before and after the application of a retrofit strategy will not only indicate the effectiveness of this strategy in improving bridge seismic performance; it will also exhibit the impact of retrofit on system functionality under regional seismic hazard.

2.1 Seismic Resilience

Past studies have defined and calculated the resilience of various lifeline systems such as acute care hospitals, water supply systems, power transmission systems and transportation systems (Chang and Nojima 2001, Bruneau et al. 2003, Chang and Chamberlin 2004, Shinozuka et al. 2004, Rose and Liao 2005, Paton and Johnston 2006, Amdal and Swigart 2010, Arcidiacono et al. 2010, Decò et al. 2013, Cimellaro 2013, Venkittaraman and Banerjee 2013, to name a few). In general, resilience is defined in these studies as a dimensionless quantity representing the rapidity of the system to revive from a damaged condition to the pre-damaged functionality level. Loss due to a natural event and post-event performance recovery of a system are its two major components. Hence, resilience R can be expressed as shown in the following equation (Cimellaro et al. 2010).

$$R = \int_{t_{0E}}^{t_{0E}+T_{LC}} \frac{Q(t)}{T_{LC}} dt \tag{1}$$

where t_{0E} represents the time when the extreme event E occurs and T_{LC} is a controlled time set to evaluate resilience. $Q(t)$ represents system functionality, which can be expressed as a dimensionless function of time t. The analytical expression of $Q(t)$, given in the following equation, constitutes a loss function and a recovery function of system performance during the period of system interruption due to the extreme event.

$$Q(t) = 1 - \left[L(I, T_{RE}) \times \left\{ H(t - t_{0E}) - H(t - (t_{0E} + T_{RE})) \right\} \times f_{rec}(t, t_{0E}, T_{RE}) \right] \quad (2)$$

Here $L(I,T_{RE})$ is the loss function, f_{rec} is the recovery function, I is seismic intensity, and T_{RE} is the recovery time for event E. $H()$ is the Heaviside Step function; this discontinuous function takes value equal to either one or zero based on positive and negative arguments. As can be seen from Equation 2, $Q(t) = 1.0$ in case of no loss and $0 < Q(t) < 1.0$ when there is loss due to seismic damage. Figure 2.1 schematically represents system functionality before and just after a seismic event and during the post-event recovery process.

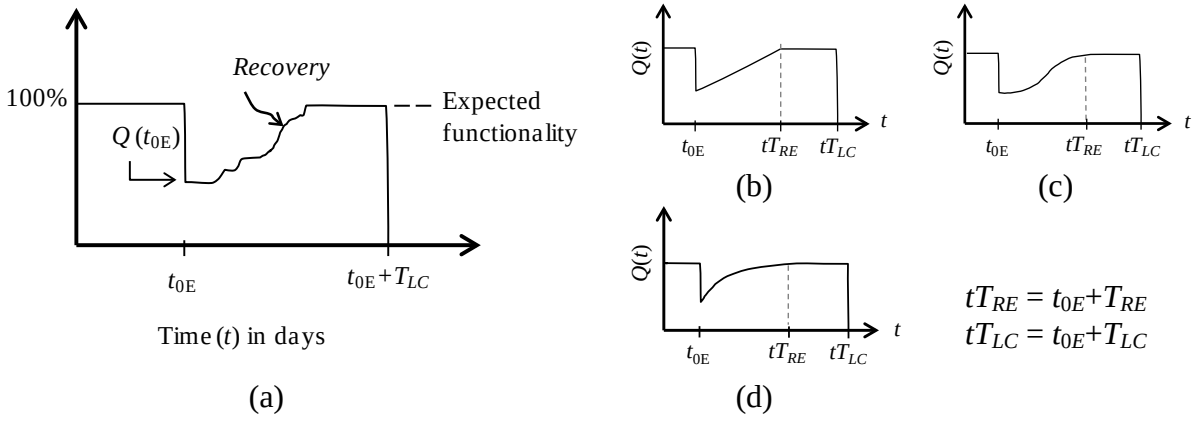

Figure 2.1: Schematic representation of disaster resilience and post-event recovery functions**;** (a) functionality curve, (b) linear recovery function, (c) trigonometric recovery function and (d) negative exponential recovery function

2.2 Fragility Function

The present study measured bridge vulnerability in the form of fragility curves. Fragility curves represent the probability of exceeding a bridge damage state under certain intensity of ground motions such as peak ground acceleration, or PGA (Banerjee and Shinozuka 2008). Two-parameter lognormal distributions are generally used to develop fragility curves. The analytical expression is given as

$$F(PGA_j, c_k, \zeta_k) = \Phi\left[\frac{\ln(PGA_j / c_k)}{\zeta_k} \right] \quad (3)$$

where PGA_j represents PGA of a ground motion j and k represents bridge damage states such as minor, moderate, major damage, and complete collapse. The two parameters c_k (median value) and ζ_k (log-standard deviation) are fragility parameters for a damage state k, estimated by maximizing the likelihood function L, as given below.

$$L = \prod_j \left[F\left(PGA_j, c_k, \zeta_k\right)\right]^{r_j} \left[1 - F\left(PGA_j, c_k, \zeta_k\right)\right]^{1-r_j} \quad (4)$$

where r_j = 0 or 1 depending on whether or not the bridge sustains the damage state k under j^{th} ground motion.

2.3 Loss and Recovery Functions

The loss function incorporates all direct and indirect losses from a post-event degraded system over the period of system restoration. The direct loss for a bridge seismic damage arises due to bridge restoration after the seismic event. It includes the cost associated with post-event repair and rehabilitation of damaged bridges or bridge components. Hence, direct loss due to a seismic event can be calculated by multiplying the occurrence probability of the event and failure probability of a system (or system component) under this event (Zhou et al. 2010, Prasad and Banerjee 2013). For a bridge, direct economic loss (C_{rE}) resulting from an event E can be evaluated in terms of a dimensionless cost term L_D that represents the ratio of restoration cost C_{rE} to replacement cost C, as

$$L_D = \frac{C_{rE}}{C} = \sum_k P_E\left(DS = k\right) \times r_k \quad (5)$$

where k represents the damage states of the bridge, P_E (DS = k) is the probability of bridge failure at damage state k during the seismic event E, and r_k is the damage ratio corresponding to damage state k. Values of P_E (DS = k) and r_k can be obtained, respectively, from bridge fragility curves developed for various damage states and HAZUS (HAZUS 1999). Replacement cost C can be evaluated by multiplying bridge deck area with the unit area replacement cost (Zhou et al. 2010).

Indirect loss (L_{ID}) arises due to the disrupted functionality of the system after an event. For highway transportation systems, indirect losses consist of rental, relocation, business interruptions, traffic delay, loss of opportunity, losses in revenue, etc. In addition, casualty losses may also be included in the indirect loss model to calculate resilience of critical care facilities such as hospitals (Cimellaro et al. 2013). Indirect losses are time dependent. These losses are at their maximum immediately after the extreme event and gradually reduce as bridge restoration takes place. Past studies of highway bridges have taken indirect loss to be 5-20 times greater than the direct loss (Dennemann 2009). A more specific value of indirect to direct loss ratio can be calculated if information on traffic flow in a highway network before and after an earthquake can be obtained and dynamic equilibrium using network capacity and traffic demand can be established (Zhou et al. 2010). Such a comprehensive traffic analysis was beyond the scope of the present study. Hence, an expected value for indirect to direct loss ratio of 13 was assumed in this study for each bridge damage state. A similar approach was adopted by Denneman (2009). Recovery time of a bridge is not a unique quantity; it greatly depends on the severity of bridge damage due to the extreme event. Zhou et al. considered that the time required to complete a bridge restoration is a random variable uniformly distributed between the maximum and minimum required times to complete the restoration job. In the seismic loss estimation manual (HAZUS 2003), recovery times for different seismic damage states of highway bridges are modeled with normal distribution functions, distribution parameters (mean and standard deviation) of which are given in Table 2.1. These distributions were originally developed based on earthquake damage evaluation data acquired for California (ATC-13 1985).

Table 2.1: Mean and standard deviation of post-seismic restoration times for highway bridges

Bridge Damage State	Slight/Minor	Moderate	Extensive	Complete
Mean (Days)	0.6	2.5	75	230
SD (Days)	0.6	2.7	42	110

2.4 Testbed Bridge

A reinforced concrete bridge in the La Cienega-Venice Boulevard sector of Santa Monica (I-10) freeway in Los Angeles, California was selected as a testbed bridge. It is a multispan reinforced concrete bridge, as shown in Figure 2.2 (schematic). Cross-sectional and material properties of bridge girder were obtained from Broderick and Elnashai (1994) and Lee and Elnashai (2002). Bent 5 is a multi-column bent with three identical piers. Bents 6 to 8 each has a single pier with the same diameter as the piers in bent 5. Based on the reinforcement used, these piers have either type 'H' (in bent 5) or type 'M' (in bents 6 to 8) cross-sections. Bent 9 has a rectangular wall section. All pier-girder connections are monolithic. There is an in-span expansion joint just after bent 6.

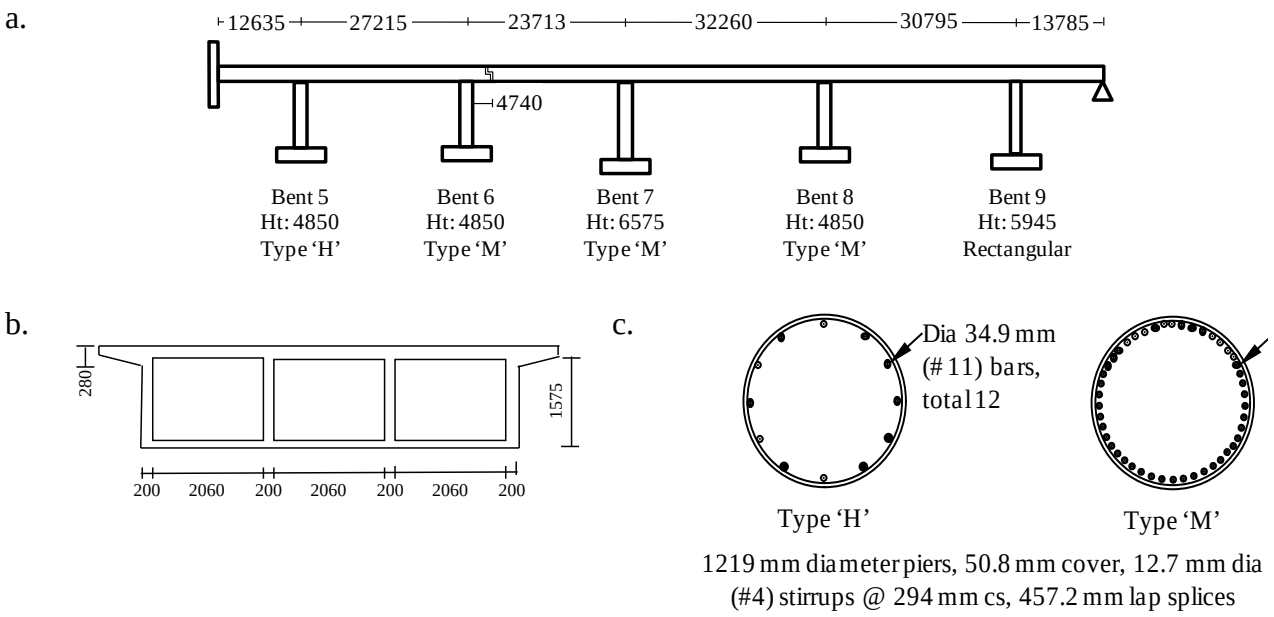

Figure 2.2: (a) The testbed bridge (schematic), (b) cross-section of bridge girder, and (c) cross-sections of type 'H' and 'M' piers (all units are in mm)

A finite element model of the bridge was developed using SAP2000. Modeling of various bridge components and their geometric and material properties are discussed next.

Bridge girder – A 140.4-m-long bridge girder was modeled using linear elastic beam-column elements, as this component of the bridge is expected to respond within the elastic range during seismic excitation.

Bridge piers – During seismic excitation, the maximum bending moment generates at pier ends. This often leads to the formation of plastic hinges at these locations when the generated moment exceeds the plastic moment capacity of these sections. To model such nonlinear behavior at bridge pier ends, nonlinear rotational springs were introduced in bridge models at the top and bottom of each pier. Rigid elements were assigned at pier ends to ensure rigid connectivity at pier-girder connections of monolithic concrete bridges. The cap beam for three piers in bent 5 was modeled as a rigid link.

In-span expansion joint – At an in-span expansion joint, the bridge is modeled such that the two ends of the expansion joint can move independently in the longitudinal direction and rotate in the longitudinal plane, while they have no relative vertical movement. The opening and closure of an expansion joint during bridge movement are modeled by assigning hook and gap elements, respectively (Banerjee and Shinozuka 2008). The hook element represents the effect of restrainer at the expansion joint and controls relative displacement (excessive separation) between two adjacent girders at the expansion joint. A non-linear link element with an initial slack of 25.4 mm was used as a hook element. Force develops in this element when the outward relative displacement of adjacent bridge decks is more than initial slack. A nonlinear gap element with an initial gap of 12.7 mm and linear elastic stiffness of 223.3 MN/m (calculated according to Cofer et al. 1997) for longitudinal translation were assigned. Hence, the gap element becomes active only when the relative inward displacement of adjacent bridge decks in the longitudinal direction of the bridge exceeds the initially provided gap width of 12.7 mm.

Foundation – Translational foundation springs are assigned at pier bottoms in the longitudinal and transverse directions of the bridge. Spring constants in the lateral direction were calculated considering

7 kN/mm lateral stiffness of each pile (Neilson et al. 2006, Caltrans 1999). Thus, lateral foundation stiffness for type 'M' and 'H' piles were calculated to be 98 kN/mm and 84 kN/mm, respectively. For the purpose of model validation, fixed condition was assumed at all pier bottoms to be consistent with the analysis performed by Broderick and Elnashai (1994). After validation, appropriate foundation models (as discussed above) were assigned to realistically capture soil-foundation interactions at bridge foundations.

Figure 2.3 shows the computed (actual) and bilinear moment-rotation envelopes of bridge piers that are developed through the moment-curvature analysis described by Priestley et al. (1996). M_y and M_u represent the yield and ultimate moment carrying capacities of pier cross-sections, respectively, and θ_y and θ_u are corresponding rotations, while $k_{elastic}$ represents the initial elastic stiffness of the member and α is the post yield stiffness ratio. Axial load levels on these piers vary from pier to pier, due to which moment-rotation relations of piers in bent 6, 7, and 8 are different, although they have the same cross-sectional and material properties.

2.5 Validation of Finite Element Model of the Bridge

For model validation, the bridge was analyzed for the two horizontal orthogonal components of the Northridge earthquake recorded at the City Hall station (in Santa Monica), which is approximately 10 km away from the bridge site. This is the nearest recording station from the bridge site amongst several others located in this region. Peak ground accelerations (PGAs) of these two components were recorded to be 0.370 g and 0.883 g, propagated along the longitudinal and transverse directions of the bridge, respectively.

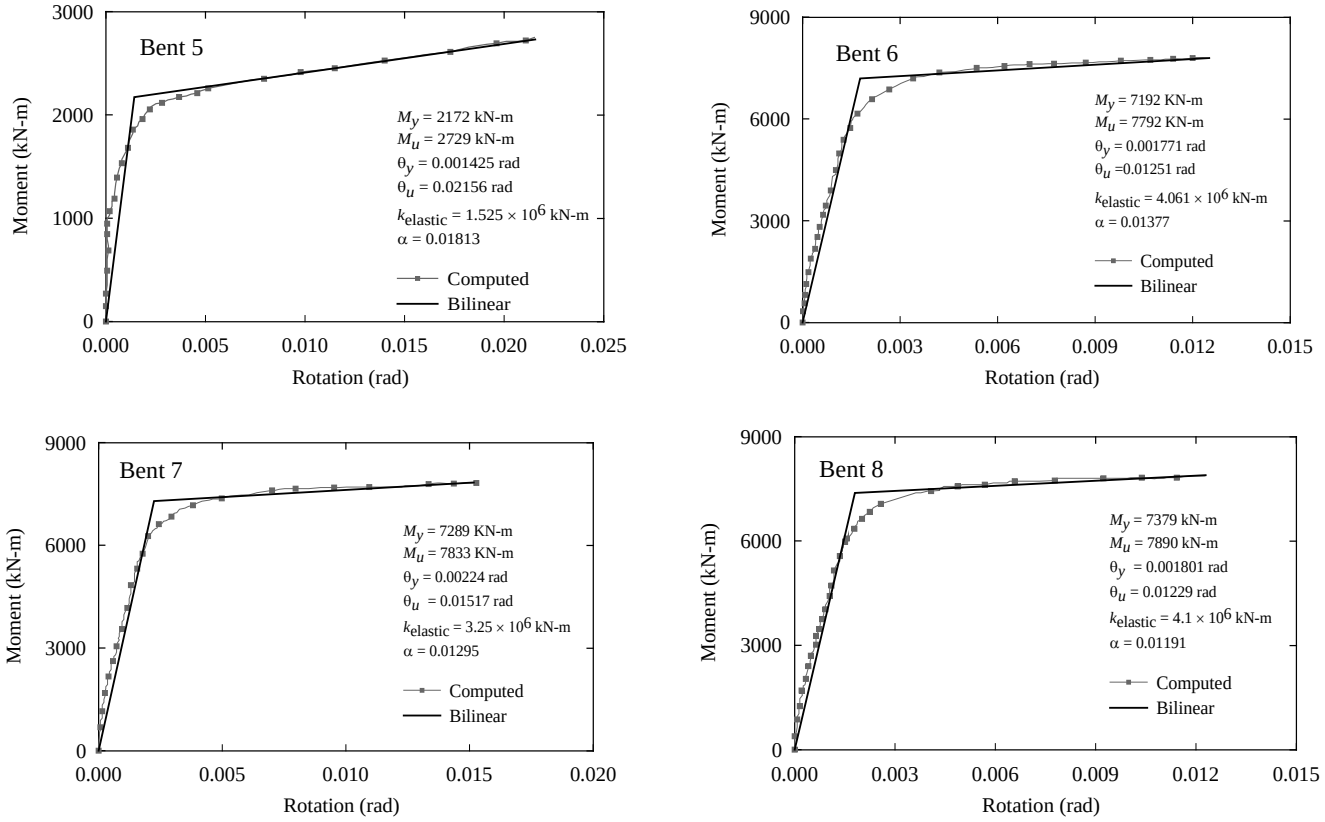

Figure 2.3: Moment-rotation diagrams of piers in bent 5 to bent 8

Fundamental time periods and mode shapes of the bridge at the first five modes are presented in Table 2.2, as obtained from the present study and Broderick and Elnashai (1994). This table depicts that obtained dynamic properties of the bridge from the present study are in good agreement with those calculated in a previous study.

Table 2.3 shows shear capacities of bridge piers in bent 6, 7, and 8 calculated following Priestley et al. (1996). These shear demands were obtained from nonlinear time history analysis of the bridge when two orthogonal components of the Northridge earthquake were applied simultaneously. Comparison of shear capacity with demand shows that the pier in bent 6 fails in shear as the demand exceeds capacity at this location. The same phenomenon is also observed during the Northridge earthquake.

Table 2.2: Comparison of modal shapes and fundamental time periods of the bridge

Modes	From the Present Study		From Broderick and Elnashai	
	Time Period	Mode Shape	Time Period	Mode Shape
1	0.44	Transverse	0.46	Transverse
2	0.29	Transverse	0.28	Transverse
3	0.24	Deck	0.20	Deck
4	0.20	Deck	0.16	Deck
5	0.18	Deck	0.16	Deck

Table 2.3: Shear capacities and shear demand at bridge piers

Location of Bridge Pier	Shear Capacity	Shear Demand	Conclusion
Bent 6	2537 KN	2540 KN	Pier in bent 6 failed in shear
Bent 7	2353 KN	2063 KN	
Bent 8	2715 KN	2362	

2.6 Bridge Fragility Curves

During the Northridge earthquake, a major horizontal ground motion component propagated along the transverse direction of the bridge, resulting in shear failure of pier in Bent 6 in this direction. Hence, the testbed bridge is most vulnerable in the transverse direction. To be consistent with the actual damage of the bridge, a seismic fragility analysis was performed by applying ground motions in the transverse direction of the bridge. Bridge seismic damage is characterized through shear and flexural failures of bridge piers. These two failure modes were assumed to govern the global failure of the bridge. Other possible seismic bridge failure modes such as unseating of bridge girders and failure at expansion joint were assumed to be non-governing failure modes. In general, shear failure of a bridge pier is brittle in nature and sometimes causes irreversible damage to bridges. Hence, such a mode of failure is considered here as ultimate damage (i.e., complete collapse) of the bridge. For flexural damage of bridge piers, HAZUS (1999) provided five different bridge damage states, namely: none, minor (or slight), moderate, major (or extensive) damage, and complete collapse. Among these, the complete

collapse state is the ultimate damage state of the bridge and others are named according to the severity of bridge seismic damage without complete collapse.

To generate fragility curves of the bridge, shear and flexural damage of the bridge were defined in a quantitative manner. Seismic damage states are ranked with k = 1 to 4, in which k = 1 represents minor damage and k = 4 represents complete collapse. If shear failure occurs due to j^{th} ground motion, the bridge is considered to have damage condition r_j = 1 at damage state k = 4. For flexural damage, bridge damage condition (r_j = 0 or 1) at a particular damage state is defined based on rotational ductility of bridge piers. By definition, rotational ductility (μ_Δ) is the ratio of rotation of bridge θ piers to the yield rotation (θ_y) measured at the same location. During time history analyses of the bridge under 60 motions, rotational time histories were recorded at both the top and bottom of all bridge piers where plastic hinges are likely to appear. Rotational ductility for each pier was obtained by dividing maximum rotations from rotational time histories with yield rotations of corresponding locations that are obtainable from moment-rotation plots shown in Figure 2.3. These rotational ductility values are considered as signature, representing the flexural response of the bridge under seismic motions.

To define the damage condition of the bridge at each damage state due to flexure under 60 ground motions, rational ductility values were compared with threshold limits. These threshold limits for each bridge damage state are shown in Table 2.4. The bridge was constructed in 1964; so, it is reasonable to assume that bridge piers were not properly designed to carry lateral loading from seismic events. The deficiency of lateral confinement in bridge piers was also evident from the post-Northridge reconnaissance report by Cofer *et al.* (1997). For this reason, threshold limits of rotational ductility for various seismic damage states of the bridge were calculated based on drift limits of non-seismically designed bridge piers recommended by HAZUS (1999). Table 2.4 shows the non-seismic drift limit ratios obtained from HAZUS for bridge seismic damage state and corresponding threshold rotational

ductilities of piers in bent 6, 7, and 8. Note that rotational ductility values of the bridge at no damage and complete collapse state are taken to be equal to the yield and ultimate rotational ductility of bridge piers, respectively. As threshold rotational ductility at ultimate state varies from pier to pier, the threshold values for intermediate damage states (i.e., minor, moderate, and major) also vary accordingly. Piers in bent 5 are excluded from this table. Piers in this multi-column bent have low probability of forming plastic hinges compared to other single-column bents of the bridge. Also, shear forces developed in piers of bent 5 were low relative to their shear capacities. Hence, bent 5 is excluded from shear comparisons as well.

Table 2.4: Drift ratios and threshold values rotation ductility

Damage States	Non-seismic Drift Ratio (HAZUS 1999)	Threshold Rotation Ductility of Bridge Piers		
		Bent 6	Bent 7	Bent 8
No damage	0.002	1.00	1.00	1.00
Minor	0.005	1.37	1.36	1.36
Moderate	0.01	2.01	1.96	1.97
Major	0.02	3.28	3.16	3.18
Collapse	0.05	7.06	6.77	6.82

For each ground motion, damage condition of the testbed bridge due to flexure is assigned by comparing rotational ductility values of bridge piers with corresponding threshold limits and seismic fragility curves are developed at the minor, moderate, major damage, and complete collapse states (Figure 2.4). HAZUS (1999) suggested an uncertainty factor for seismic demand to be equal to 0.5 (Pekcan 1998). Following this, ζ_k is taken here as 0.5 for all damage states. This common ζ_k for all damage states restricts the intersection of any two fragility curves (Shinozuka et al. 2000). These fragility curves indicates that the testbed bridge has 100%, 99.7%, 95.3%, and 93.5% failure probabilities respectively in minor, moderate, major damage, and complete collapse states due to the transverse component of the Northridge earthquake (with PGA of 0.883 g). These high probabilities of

failure indicate extensive damage of the bridge due to the Northridge earthquake. Thus the fragility curves can appropriately simulate the seismic vulnerability of the bridge.

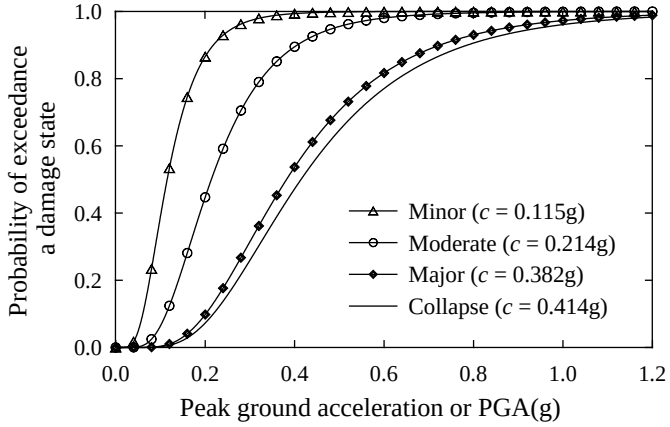

Figure 2.4: Seismic fragility curves of the testbed bridge at four damage states

2.7 Direct and Indirect Losses due to the Northridge Earthquake

The direct loss due to bridge damage during the Northridge earthquake was calculated following Equation 5. Damage ratios (r_k) at minor, moderate, major, and complete collapse states of the bridge are, respectively, 0.03, 0.08, 0.25, and 2/span number as specified by HAZUS (1999). An overall cost ratio of 0.96 was obtained due to direct and indirect losses from the Northridge earthquake. A sensitivity study was performed toward the end of this study by taking various ratios of indirect to direct losses.

2.8 Seismic Resilience

Seismic resilience of the bridge due to the Northridge earthquake was calculated using Equations 1 and 2. Information on bridge seismic vulnerability as obtained from fragility curves (Figure 2.4) was combined with post-event loss and recovery functions. Percentage values of bridge seismic resilience were calculated to be 57.47%, 99.92%, and 57.69%, respectively, when linear, negative exponential, and trigonometric recovery functions were considered. According to these values, linear and trigonometric

recovery models result in approximately the same resilience of the bridge, whereas the negative exponential recovery function results in very high resilience of the testbed bridge, even if the bridge experienced severe damage. In reality, the rate of initial recovery is not extremely fast as an exponential function because of post-event reconnaissance, damage assessment, and planning to initiate rehabilitation before which the recovery process cannot be started. Hence, a negative exponential recovery model for all bridge damage states is far from reality and not applicable for most of the real-life disaster scenarios. Therefore, the linear recovery function is used for the remainder of this report (Zhou et al. 2010).

2.9 Bridge Seismic Retrofit and Enhancement in Resilience

Steel jackets have been used as a retrofit measure to enhance the flexural ductility and shear strength of reinforced concrete bridge piers. These are typically steel casings that are applied to bridge piers keeping a space of about 50.8 mm at pier ends to prevent the jacket from bearing on adjacent members. The full length of bridge piers in bent 6, 7, and 8 were jacketed with 0.4-mm-thick steel jackets. The jacket thickness was decided based on practical consideration of handling the jacket during retrofit operation. Due to jacketing, moment-rotation behaviors of retrofitted piers were improved (shown in Figure 2.5), which resulted in enhanced rotational ductility of the bridge piers.

To develop a seismic vulnerability model of the retrofitted bridge, time history analysis of the bridge was performed under the same set of 60 ground motions. It was observed that among 60 cases, only 8 cases exhibited minor damage due to flexure. No higher flexural damage (such as moderate, major, or complete collapse) was observed. Also, no shear damage was observed in any of the retrofitted bridge piers. To confirm the observation, another method proposed by Sakino and Sun (2000) to calculate shear capacity of jacketed concrete bridge piers was used and high values of shear capacity of bridge piers were obtained (Venkittaraman 2013). Based on this damage scenario, the

fragility curve of the retrofitted bridge was developed only at the minor damage state (Figure 2.6). The median value of the fragility curve was estimated to be 1.27 g with a log-standard deviation of 0.5.

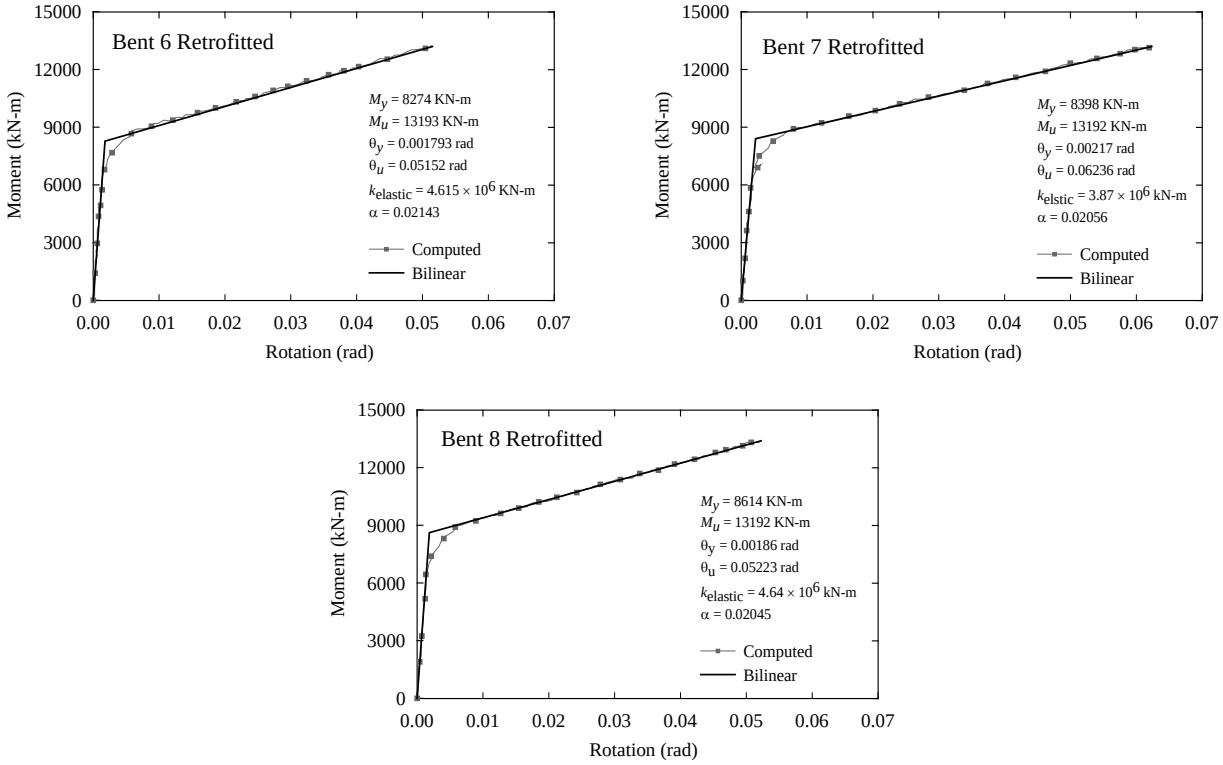

Figure 2.5: Moment-rotation diagrams of retrofitted piers in bent 6, 7 and 8

Due to the strong seismic fragility characteristics of the retrofitted bridge, an overall loss ratio of 0.09 was calculated for this bridge under the Northridge earthquake. A linear recovery function with an appropriate model for recovery time was considered to calculate seismic resilience. Results show 99.97% resilience of the bridge under the Northridge earthquake if the bridge were retrofitted with steel jacket prior to the event. Hence, a 74% increase in seismic resilience of the bridge was observed due to seismic retrofitting.

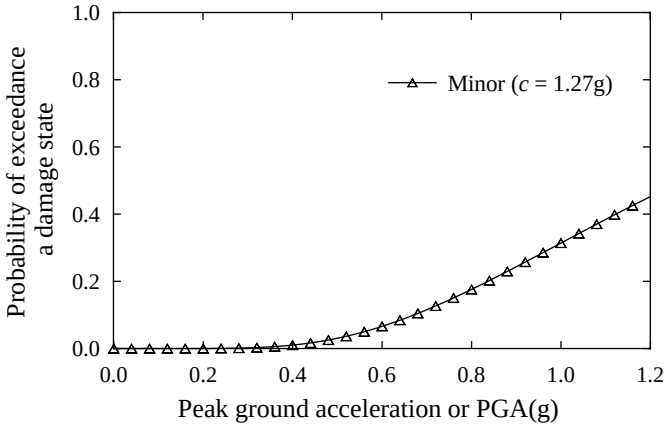

Figure 2.6: Fragility curves at minor damage state of the retrofitted bridge

3. SENSITIVITY ANALYSIS AND UNCERTAINTY ANALYSIS

It was recognized that the uncertainties involved with various parameters in the resilience calculation module could introduce uncertainty in the calculated resilience. A sensitivity study was performed to analyze the impact of various uncertain parameters on seismic resilience. For this, the Northridge earthquake is considered as the scenario event for which bridge resilience is estimated. As retrofitting resulted in very high resilience under this scenario event, it would not be possible to distinguish any positive impact of uncertain parameters on seismic resilience if the sensitivity study were performed on the retrofitted bridge. Thus the un-retrofitted (original) bridge was used for the sensitivity analysis. Although the original bridge is too vulnerable under the Northridge earthquake, estimated resilience of the bridge is 57.47% when a linear recovery function is used. This value is the most expected value of resilience when mean values of all input parameters are considered. Due to uncertainty in input parameters, a distribution of resilience will be observed on both sides of the most expected value of resilience. Note that the observation made from this sensitivity study will be restricted to the case study performed here and may not be applicable to any bridge and seismic event in general.

3.1 Uncertain Parameters

The study considered recovery time, control time, indirect-to-direct loss ratio, and bridge fragility parameters (median values) to be the uncertain parameters. These parameters are statistically independent. Other parameters in the analysis module were considered to be deterministic and their values were kept fixed. For sensitivity study, each uncertain parameter was varied individually while keeping all other parameters at their respective mean values. A linear recovery function was used to calculate resilience for each case.

(i) Recovery time: To observe the sensitivity of seismic resilience to recovery time, T_{RE} at different bridge damage states were considered to have normal distributions (Table 2.1). The as-built bridge

had shear failure during the Northridge earthquake. Consequently, a normal distribution with a mean value of 75 days and standard deviation of 42 days was used to model the uncertainty of recovery function for the as-built bridge. Seismic resilience of the bridge was calculated for mean ± standard deviation of the recovery time.

(ii) Control time: In general, the control time T_{LC} is decided by engineers or bridge owners. It depends on the time window of interest, and thus it can be greater or less than the recovery time. The resilience of the as-built bridge was calculated for mean ± standard deviation of the control time to calculate its influence on bridge resilience. In the present study, the control time was assumed to have a normal distribution with a mean value and standard deviation of 85 days and 40 days, respectively.

(iii) Indirect to direct loss ratio: The indirect to direct loss ratio may vary between 5 and 20 (Dennemann 2009). Even higher variation can be observed based on important physical and decision-making parameters including system redundancy, population type and density, preparedness for post-event recovery, and fund allocation. The present study considered the most expected value of indirect to direct loss ratio to be 13 with a standard deviation of 8. With this, the entire range of indirect to direct loss ratio as stated in (Dennemann 2009) was covered.

(iv) Fragility parameters: Fragility parameters of the bridge may vary due to uncertainty of parameters pertaining to the structure and ground motions. A detailed uncertainty analysis considering all uncertain bridge and ground motion parameters was beyond the scope of the present study. For this reason, variability (or uncertainty) of fragility curves was quantified in terms of 90% confidence intervals (between 5% and 95% confidence levels) of these curves. This was a reasonable approach to model the uncertainty associated with fragility curves in the absence of any detailed uncertainty quantification analysis. Fragility parameters at 95% and 5% confidence levels

(with 95% and 5% exceedance probabilities, respectively) were estimated following the procedure described in previous studies (Banerjee and Shinozuka 2008, 2009). Fragility parameters with 95%, 50%, and 5% confidence bands are listed in Table 3.1.

Table 3.1: Fragility parameters with 90% confidence intervals

Damage State	Median Fragility Parameter (g)		
	95% confidence	50% confidence	5% confidence
Minor	0.101	0.115	0.130
Moderate	0.197	0.214	0.234
Major	0.356	0.382	0.407
Collapse	0.389	0.414	0.441

3.2 Methods for Sensitivity Analysis

A first-order, second-moment reliability analysis was performed for this sensitivity study. In this, the resilience of the as-built bridge was considered to be the performance function. The value of resilience was calculated for mean ± standard deviation of each uncertain parameter. When one parameter is varied, values of other uncertain parameters are kept at their respective mean values. The analysis provides relative variances which can be defined as the ratio of variance of resilience due to i^{th} random variable to the total variance of resilience due to all random variables (Ang and Tang 1984). In other words, relative variance represents the relative contribution of each uncertain parameter to the total uncertainty of resilience. Hence, values of relative variance indicate the influence of each random variable on the performance function. Figure 3.1 shows the relative variance for each uncertain parameter. As the figure shows, the recovery time T_{RE} and control time T_{LC} have the major influence on seismic resilience of the bridge. Uncertainties in indirect to direct loss ratio and bridge fragility have no influence on resilience.

A tornado diagram, shown in Figure 3.2, was also developed to represent the hierarchy of uncertain parameters for seismic resilience of the bridge (Banerjee and Prasad 2013). The center dotted

line in the diagram represents the most expected value of resilience (equal to 57.47%) when mean values of all uncertain parameters were considered. Swings of resilience on both sides of the dotted line show variations of seismic resilience for mean ± standard deviation values of each uncertain parameter. The longer the swing, the higher is the influence of the corresponding input parameter on the output. Again, each parameter was varied independently, keeping all other parameters at their respective mean values. This tornado diagram shows the same hierarchy as seen from FOSM, and hence confirms the sensitivity of seismic resilience on recovery time and control time.

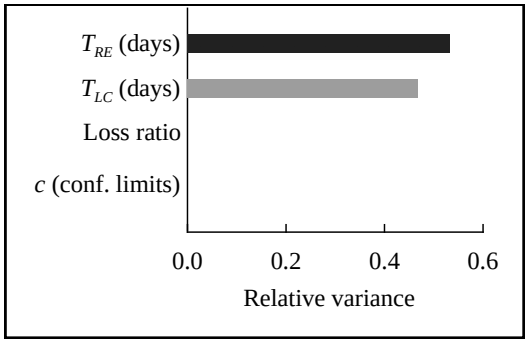

Figure 3.1: Relative variance of uncertain parameters

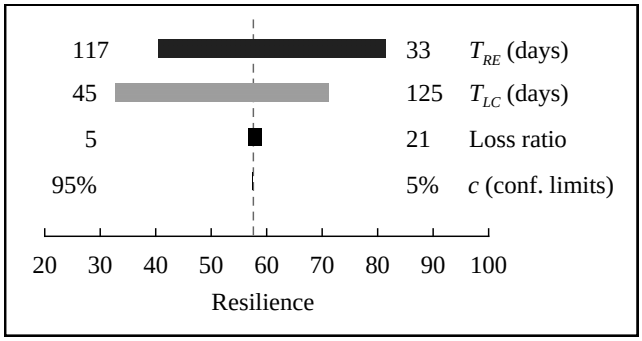

Figure 3.2: Tornado diagram with uncertain parameters

3.3 Uncertainty of Seismic Resilience

It is evident from Figure 3.2 that seismic resilience is directly proportional to T_{LC} and inversely proportional to T_{RE}. Figure 3.3 shows independent influences of T_{RE} and T_{LC} on the variation of seismic resilience R. In this figure, the variation of R with T_{LC} is obtained when T_{RE} is kept at its mean value (= 75 days). Similarly, T_{LC} is set to its mean value (= 85 days) when the variation of R with T_{RE} is obtained. As the figure shows, resilience varies linearly with T_{RE} and T_{LC} until $T_{RE} = T_{LC}$ (points A and B on the figure). Beyond this, resilience has nonlinear variations with these parameters. The linear trend is obvious, as a linear recovery function was used to evaluate resilience for the sensitivity study.

The value of resilience would eventually reach to an asymptotic value if T_{LC} and T_{RE} were increased further beyond their maximum values shown in the figure.

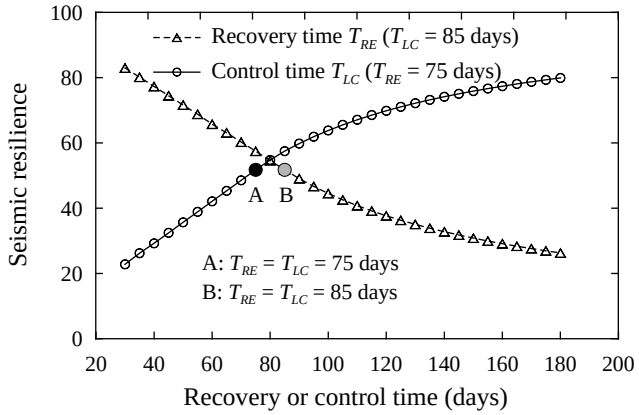

Figure 3.3: Variation of resilience with recovery time T_{RE} and control time T_{LC}

To observe the uncertainty in seismic resilience of the bridge under the Northridge earthquake, the Latin Hypercube random sampling technique (McKay 1992) was used to generate random combinations of T_{RE} and T_{LC}. The advantage of this sampling technique is the randomness in data selection, such that not a single data point was repeated to form combinations. Normal distributions of T_{RE} and T_{LC}, as discussed in Section 6.1, were used for random sampling. The range of each random variable was divided into 4 equally probable intervals that resulted in 24 random combinations of T_{RE} and T_{LC}. For each combination, seismic resilience was estimated and observed to have a wide-ranging variation, from 17% to 99%. To estimate the uncertainty associated with these resilience values, a suitable random distribution was assigned to describe the statistical nature of seismic resilience. A goodness-of-fit test revealed that a normal distribution cannot be rejected at significance levels of 0.10 and 0.20 to define seismic resilience. The mean, standard deviation, and coefficient of variation of the normal distribution are 53.73, 23.98, and 45%, respectively. This high uncertainty in seismic resilience is the result of high variations considered in recovery and control times. The distribution is further

verified by plotting resilience values in a normal probability paper (Figure 3.4 (a)). Figure 3.4 (b) shows the cumulative distribution function (CDF) of the normal distribution and 24 values of resilience generated through random sampling of T_{RE} and T_{LC}. As the figure shows, the 24 generated values of resilience cover 92% probability (between 4th and 96th percentile values), which is nearly ±2 times the standard deviation of the normal CDF.

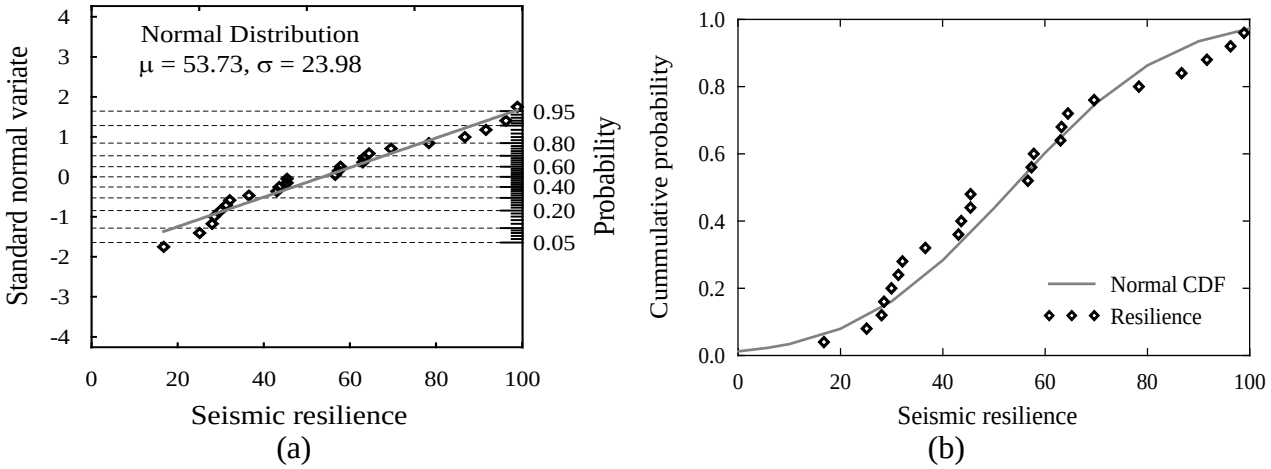

Figure 3.4: Uncertainty in seismic resilience of the bridge estimated for the Northridge earthquake; (a) normal probability paper and (b) normal CDF

Note that the quantification of uncertainty of seismic resilience due to uncertain T_{RE} and T_{LC} is the focus of this section. It was realized that very low value of T_{LC} compared to T_{RE} might not be practically possible, and hence all values of resilience as obtained through the random sampling of T_{RE} and T_{LC} might not be realistic to the testbed bridge. However, all combinations of T_{RE} and T_{LC} were considered in the study for the completeness of uncertainty analysis. Furthermore, the nature of obtained distribution of resilience and distribution parameters could change if different distributions of T_{RE} and T_{LC} were considered. Hence, the quantified uncertainty in seismic resilience may not be generally applicable to any bridge and damage scenario.

4. COST-BENEFIT ANALYSIS

Through the calculation of seismic resilience, this study showed that the failure and associated losses of the as-built bridge could have been avoided if the bridge piers had been retrofitted with steel jackets prior to the Northridge event. In this relation, it is also important to justify the cost associated with seismic retrofitting. A cost-benefit analysis was performed here in which the cost of retrofit and benefit from retrofit were calculated. If calculated benefit is more than cost of retrofit, the retrofit strategy is regarded to be cost-effective.

4.1. Cost of Retrofit

The cost of retrofitting three bridge piers in bents 6, 7, and 8 using steel jacket was determined using the information of the California Department of Transportation's contract cost database. The cost for such a bridge retrofit type was calculated based on the weight (lb) of concrete of the element to be jacketed. From historic bid data, unit cost price for retrofit with steel jacket was found to be \$2/lb. With this, the total cost of retrofit of three bridge piers was calculated to be \$168,800.

4.2. Benefit from Retrofit

Bridge retrofit helps reduce bridge damage and costs due to direct and indirect losses after a seismic event. The expected reduction in loss is considered to be the benefit from the seismic retrofit. Thus the annual benefit, $\overline{B}$, due to seismic retrofit can be expressed as (Zhou et al. 2010):

$$\overline{B} = \sum_{m=1}^{M} \left[\left(C_{dm}^{0} - C_{dm}^{R} \right) + \left(C_{im}^{0} - C_{im}^{R} \right) \right] p_m \tag{6}$$

where C_{dm}^{0} and C_{im}^{0}, respectively, are the direct and indirect losses that arise due to earthquake *m* from the non-retrofitted bridge, while C_{dm}^{R} and C_{im}^{R} represent the same quantities from the retrofitted bridge.

M represents regional scenario earthquakes that the bridge may experience during its service life, and p_m is the annual occurrence probability of these scenario events.

The area of Los Angeles has several active seismic faults that are capable of producing hundreds of earthquakes in the future. For seismic risk assessment, Chang et al. (2000) performed a probabilistic seismic hazard analysis and developed a set of 47 scenario earthquakes that realistically represent the seismic hazard of the Los Angeles region. These 47 scenario earthquakes were used here to calculate benefit from bridge retrofit. To predict possible damage of the bridge (before and after retrofit) due to these scenario seismic events, PGAs of these events at the bridge site were estimated using attenuation relation given by Abrahamson and Silva. These PGA values were used to predict probabilities of bridge damage at various damage states with the use of fragility curves. Calculated probabilities of bridge damage were further used to compute direct and indirect losses before and after bridge retrofit and put into Equation 6 to calculate annual benefit. Thus the difference in cost, as calculated from Equation 6, is the cost avoidance due to seismic retrofit and is expressed here as an annual benefit from retrofit.

The annual benefit from retrofit cumulates over the service life of the bridge. Assuming that the design service life of the test-bed bridge was taken to be equal to 75 years when it was designed in 1964 and the retrofit was applied in 1994 prior to the Northridge event, the retrofitted bridge could serve at least another 45 years. Over this remaining service life of the bridge, total benefit B was calculated using a uniform series (Zhou et al. 2010) as given in the following equation.

$$B = \overline{B}\,\frac{(1+v)^T - 1}{v(1+v)^T} \tag{7}$$

Here, $\overline{B}$ is the annual benefit of the seismic retrofit as obtained from Equation 6, v is the discount rate, and T is the remaining service life of the bridge after retrofit. For analytical purpose, T was varied

between 30 and 50 years. The total benefit from bridge retrofit was calculated using two discount rates of 3% and 5%.

4.3. Benefit-Cost Ratio

The total benefit was divided by cost of retrofit to calculate benefit-cost ratio. Table 4.1 represents benefit-cost ratios of seismic retrofit. As can be seen, the benefit-cost ratio is more than one for all cases considered here, which indicates that the retrofit is cost-effective in general. A higher bridge service life results in more cost-effectiveness, whereas the higher discount rate yields less cost-effectiveness of bridge seismic retrofit.

Table 4.1: Summary of benefit-cost ratio

Discount rate (v)	Service life (years), T		
	30	40	50
3%	1.82	2.14	2.38
5%	1.42	1.59	1.69

5. RESILIENCE UNDER MULTIHAZARD SCENARIO

5.1. Multihazard Scenario for Bridges

Among several possible combinations of extreme hazards, earthquake in the presence of flood-induced scour is a critical multihazard scenario for highway bridges located in seismically active, flood-prone regions (Prasad and Banerjee 2013). Consequently, the present research considered the cumulative effect of earthquake and flood for bridge infrastructures. A bridge at Sacramento, CA, was selected to pursue the study. A detailed discussion on this bridge is provided later.

5.1.1. Seismic Hazard

Sixty ground-motion time histories with exceedance probabilities of 2%, 10%, and 50% in 50 years were considered to represent seismic hazard at the bridge site. Further discussion of these ground motions is given in Section 2.6 of this report.

5.1.2. Flood Hazard

Flood hazard of the study region is expressed in the form of a flood hazard curve that provides probability of exceedance of annual peak discharges in a region. Flood-frequency analysis (Gupta, 2008) is performed to develop the flood hazard curve for the study region. Annual peak discharge data recorded for Sacramento County over the past 104 years (1907–2010) were collected from the United States Geological Survey (USGS) National Water Information System (USGS, 2011). These flood data were ranked and then plotted in a log-normal probability paper to obtain the flood hazard curve of the study region (Figure 5.1). Based on HEC-18 (Richardson and Davis, 2001), the Federal Highway Administration (FHWA) design guideline mandates that all bridges over water must be able to withstand the scour associated with 100-year floods (i.e., flood events with 1% annual probability of exceedance). The same frequency of flood events has also been adopted as the base-flood by FEMA for floodplain

management purposes (FEMA, 2008). Reviewing historic flood events in the Sacramento region and following the national standards given by FHWA and FEMA, 100-year flood events are considered to be the worst flood scenario for the study region.

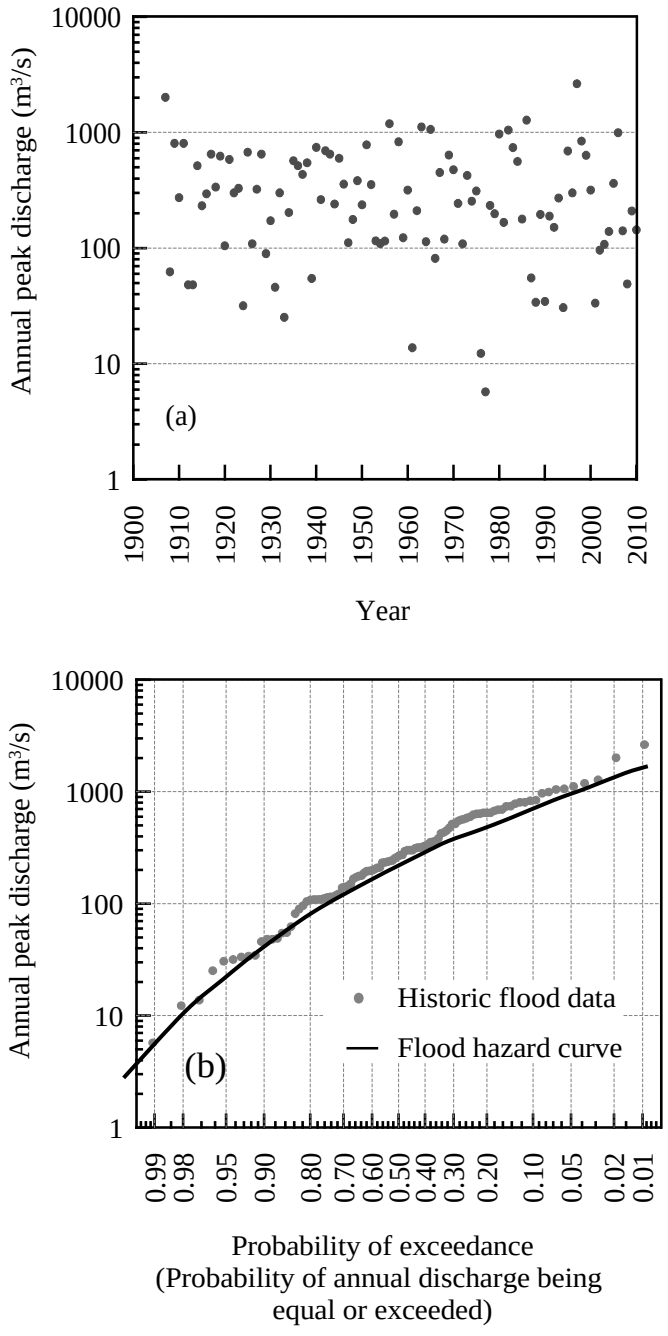

Figure 5.1: Regional flood hazard for Sacramento County in CA; (a) historic flood data and (b) flood hazard curve

5.2. Identification of Optimal Bridge Retrofit Strategy for Multihazard

For risk mitigation of bridges under this multihazard condition, the present study identified cost-effective retrofit strategies for bridges through multi-objective optimization of disaster resilience. From decade-long research, it has been identified that confinement of bridge columns using wrap-around jackets has a positive impact on seismic resistance, owing to enhanced shear and flexure capacity of bridge columns (Priestley et al. 1996, Haroun and Elsanadedy 2005). A variety of materials, including steel and FRP composites, have been popularly used for column jacketing, each of which has a different associated retrofit cost and required thickness based on its mechanical properties and demand from natural hazards. Therefore, the variable design parameters for jacket design in the present optimization study included choice of jacket material (A 36 Steel, CFRP, GFRP) and thickness of jacket. Superior designs are associated with higher cost of retrofit and vice versa. The mechanical properties of Carbon FRP are generally the best, followed by Glass FRP, followed by steel. The associated design thicknesses obviously follow the order, the lowest being that of CFRP.

5.2.1 Multi-Objective Optimization Program

In any multi-objective problem, the presence of conflicting objectives implies that there is no absolute single best solution, but a suite of solutions in which none can be explicitly said to be superior to any other in the absence of further information on preference. Multi-objective evolutionary algorithms offer an efficient and effective means to obtain a near "Pareto-optimal" set of solutions. These solutions, collectively known as Pareto front, are superior to every solution outside of their set but cannot dominate each other on one objective without becoming inferior on another. As schematically shown in Figure 5.2, a Pareto optimal set can be obtained based on objective functions 1 and 2 plotted along *x* and *y* axes. Solutions are represented in the plot with discrete points (circles, triangles, and diamonds). As the figure shows, solutions presented with open circles have better fitness than all other solutions, since

they hold lesser values on both *x* and *y* axes. Further, every open circle is better than every other open circle in terms of one and only one objective. Hence, they are similarly ranked.

One of the major distinctive features of NSGA II as compared to its predecessors is the incorporation of elitism. This means that the algorithm has a way of archiving every good solution in its search history that aids the search toward high-fitness solutions. A population-based search procedure is adopted by the algorithm to identify the most enterprising set of parameter values in order to achieve the multi-objective minimization. There are two strategy attributes to the global optimal search – "exploration" and "exploitation." As the names suggest, the former governs the tendency of the algorithm to create diverse solutions and the latter takes care of arriving at the closest-to-optimal solution within the set time and search space. The user can induce diversity by increasing the population size and the recombination rate. On the other hand, a quick convergence may be forced by restricting the number of generations if reasonably fit, but non-global optima would suffice. Using the algorithm-generated retrofit parameters, ground motion time analyses of the example bridge are performed and the resilience objective is evaluated for each set of randomly combined design parameters (i.e., for the member of population pool). Once the objective array for every member in a generation is filled up, the variable values for the subsequent generations are generated based on memory of past solutions. In this manner, the algorithm proceeds to recognize the "sweet spots" in the variable domain.

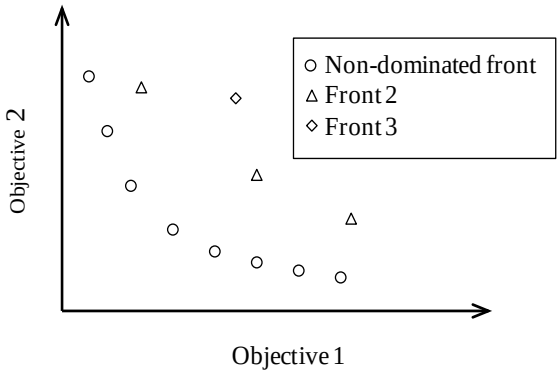

Figure 5.2: Pareto-optimal set of solutions

For each retrofit design option, nonlinear time history analyses of the bridge were performed interactively with the optimization algorithm in order to search for optimal parameter set(s) from the parameter space to generate retrofit configurations that maximize resilience and minimize the cost of retrofit. The optimization process is illustrated in Figure 5.3. The two-objective minimization problem is formulated as follows

$$\begin{aligned} &Minimize: OBJ = \{O_1\ O_2\} \\ &th_i \in [0, 25.4\,\text{mm}] \text{for steel jacket} \\ &th_i \in [0, 2.54\,\text{mm}] \text{for composite jacket} \\ &\text{and}\ \ j \in \{1, 2, 3\} \end{aligned} \tag{8}$$

Objectives array $\{O\}$ constitutes the objective functions to be minimized, O_1 and O_2 referring to the negative of resilience and cost of retrofit, respectively. The resilience objective is taken to be negative to suit the minimization problem (that actually maximizes the resilience). The parameter array consists of a number of variables corresponding to material label of the applied jacket and its thickness values for each column of a bridge.

Jacket thickness varies from 0 to 25.4 mm for steel and from 0 to 2.54 mm for carbon fiber and E-glass fiber composites where zero jacket thickness indicates no retrofit of bridge columns. $\{th_i\}$ refers to the sub-array consisting of thickness values of jackets and $\{j\}$ represents the material label: (1) steel, (2) carbon fiber composite, and (3) glass fiber composite. Results from the optimization, called a Pareto-optimal set, include solutions with the same value of overall fitness and are yet distinct from each other in terms of associated cost, contribution to resilience enhancement, and values of design parameters. Hence, this optimal set will offer the best search results in terms of design configuration based on available options for jacketing.

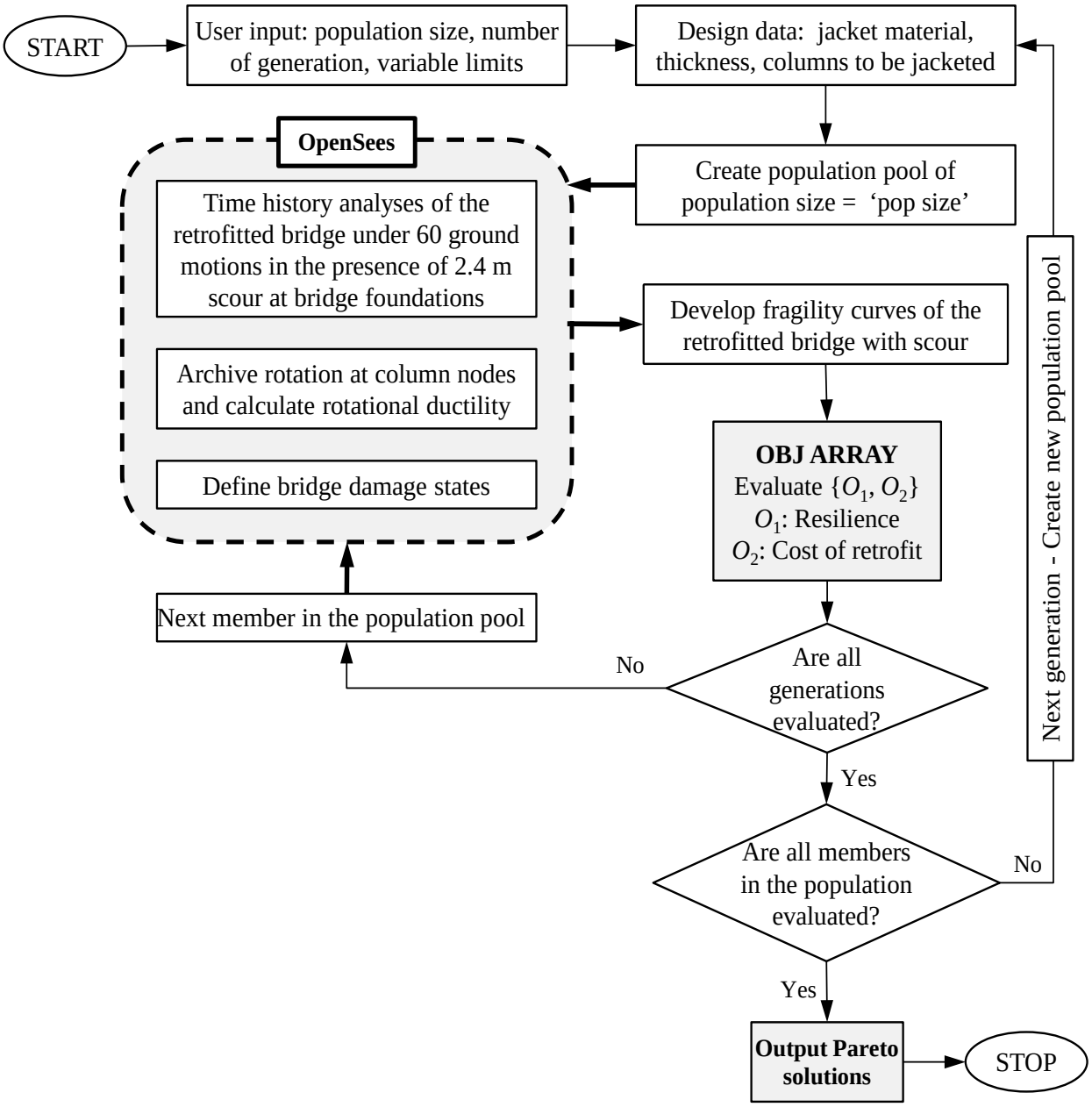

Figure 5.3: Flowchart of multi-objective optimization for retrofit design of bridges under multi-hazard

5.2.2 Mechanical Properties of Selected Retrofit Materials

Based on the implicit trade-off involved in making a decision on the choice of material for column jacketing, it was of interest to formulate a multi-objective optimization problem to understand the cost-benefit characteristics of different materials. For the purpose of this study, the three adopted materials,

steel, carbon fiber composite, and E-glass fiber composite were chosen for column jacketing. The ultimate tensile strength and Young's modulus for steel were taken to be equal to 250 MPa and 200 GPa, respectively. The same properties are 4,168 MPa and 231 GPa for carbon fiber composite and 744 MPa and 36.5 GPa for E-glass fiber composite (Haroun and Elsanadedy 2005).

5.2.3 Cost Objective

In the optimization process, one of the objectives is to minimize the cost of retrofit. Seismic bridge retrofit with both steel and composite jackets may show cost-effectiveness if a cost-benefit study is performed considering certain service lives of retrofitted bridges. However, in practice the initial retrofit cost is one of the governing factors to decide the bridge retrofit option and retrofit prioritization. The unit cost of steel was taken at a typical value of $600 per ton. The cost of retrofit using carbon jackets was estimated based on a unit cost of $37.12 per area (in ft^2) as obtained from the Contract Cost Data of the California Department of Transportation (Caltrans 1997). Effective layer thickness was assumed to be 0.0065 inch based on Caltrans bridge standard details for column retrofit using composite jackets (Caltrans 2011b). The cost of retrofit for composite jacket was calculated by multiplying the number of composite layers with the cost per unit area and the net jacketed area. For jacketing with prefabricated E-glass composite, Caltrans suggested a minimum shell thickness of 2.54 mm for composite shells to be applied to a column of diameter up to 1.83 m (Caltrans 2011c). Based on the manufacturing cost breakdown for glass and carbon fiber, the cost per unit area of glass fiber was assumed to be about 65% of the carbon fiber manufacturing cost. Thus, a unit cost of $25 per area (in ft^2) was considered for E-glass composite for the optimization study.

5.3. Model of a Case Study Bridge

The bridge model used in this study was adopted from a five-span (two 39.6-m exterior spans and three 53.3-m interior spans) RC bridge model presented by Sultan and Kawashima (1993). The bridge was

designed following the Caltrans bridge design specifications and was used to compare Caltrans and Japanese methods of seismic bridge design. The bridge deck was composed of 2.1 m deep and 12.9 m wide hollow box-girders resting on seat type abutments on either side. The hollow box girder was monolithically supported on single circular column bents, each having identical circular columns of 19.8 m length and 2.4 m diameter. A schematic elevation view of the bridge, with sectional views of the girder and columns, are shown Figure 5.4.

Finite element (FE) software *Open System for Earthquake Engineering Simulation* (OpenSees; McKenna and Fenves 2012) was used in this study. The bridge girder was modeled using linear elastic beam-column elements, as this bridge component was expected to respond within the elastic range during seismic excitations. These beam-column elements were aligned along the center line of the bridge deck. Bridge columns were modeled using nonlinear, displacement-based beam-column elements with distributed plasticity (Figure 5.4d). Rigid links were used to represent monolithic connection between bridge girder and column top. In the present study, both abutments were modeled with bilinear spring systems. In the longitudinal direction of the bridge, an initial gap of 25.4 mm was provided between the bridge girder and the abutments, and the stress-strain behavior during the closure of the gap was modeled using the ElasticPPGap spring element. In the transverse direction of the bridge, shear keys were modeled as per the capacity design principle adopted by Caltrans (MTD 5-1 1992). A single large-diameter (pile diameter is equal to the column diameter), 18.3-m-long augered pile was used as the foundation below each bridge column. Nonlinear pile-soil interaction was modeled using *p-y* springs assigned along the length of the pile.

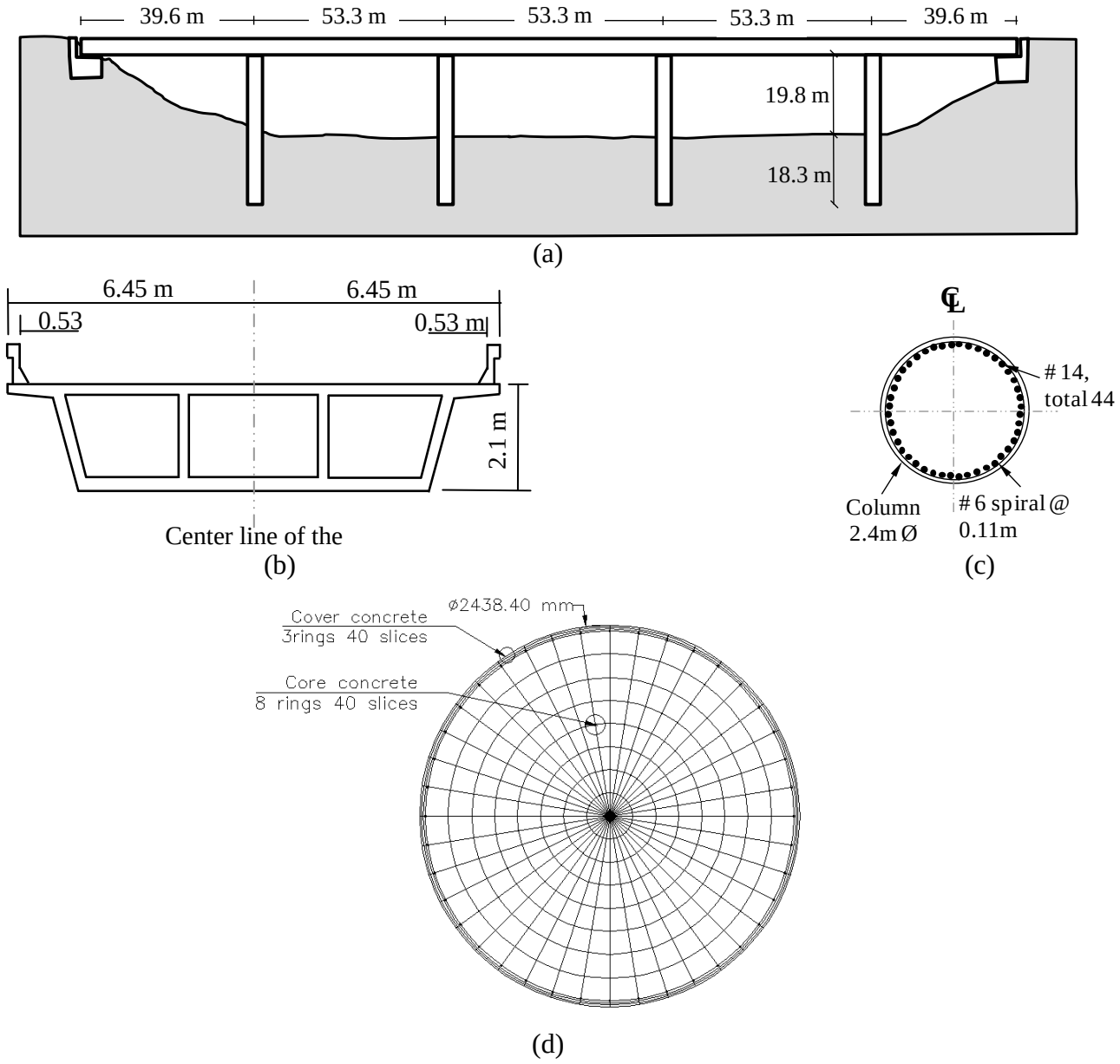

Figure 5.4: (a) Schematic of the case study bridge, (b) girder cross-section, (c) column cross-section, (d) displacement-based fiber element of column cross-section in OpenSees

The extent of flood impact on bridges is commonly measured in terms of scour depth at bridge foundation locations. Based on the physical description of subsurface soil profile given by Sultan and Kawashima (1993), a bridge site is considered to have three soil layers: a top layer of silty sand down to a depth of 11.5 m, a layer of silt between 11.5 m and 17 m, and a sand layer below 17 m. At each pier

location, the top of the pile cap is assumed to be at the ground surface level. Following this observation, scour depths considered in the present study were measured from the top of the pile cap.

Scouring at a bridge site consists of three components: (*i*) *local scour* that occurs at bridge foundations, (*ii*) *contraction scour* that occurs when normal stream flow gets obstructed (and thus contracted) by external objects, and (*iii*) long-term *aggradation and degradation scour* which is a long-term effect of continuous flow of water (Richardson and Davis 2001). Among these three components, local scour at bridge piers was considered in this study to be the expected bridge scour resulting from flood events. Depth of local scour Y_s at bridge piers was calculated using the HEC-18 guideline (Richardson and Davis 2001) and was shown in Table 5.1 for six different intensity flood events in the study region.

The present study considered a scour depth of 2.4 m at all bridge foundations. The multihazard scenario was considered such that the bridge was exposed to the flood event (that resulted in 2.4 m foundation scour) prior to the occurrence of any seismic event. Hence, the seismic vulnerability of the bridge may get enhanced due to the scour at bridge foundations.

Table 5.1 Calculation of scour

Flood Event		1.1-year	2-year	10-year	20-year	50-year	100-year
Exceedance Probability		0.90	0.50	0.10	0.05	0.02	0.01
Discharge Rates, Q (m^3/s)		60	305	900	1300	1900	2200
Local Scour Y_s (m)	5-span	0.73	2.16	2.84	3.11	3.42	3.55

5.4. Retrofit Design Domain

The optimization algorithm applied for the case study bridge consists of 5 variables (one for the jacket material and four for jacket thicknesses) with each taking discrete values from the provided domain. As

mentioned earlier, the material label takes integer values 1, 2, and 3 pertaining to steel, carbon fiber composite, and glass fiber composite, respectively. The other four variables take floating point values for individual jacket thicknesses applied to four bridge columns. The possible thickness values in mm for steel jacket are {5.1 10.2 15.2 20.3 25.4} and the same for composite jackets are {0.51 1.02 1.52 2.03 2.54}. These discrete values of jacket thickness were considered in order to avoid additional computational burden of using continuous thickness of jackets.

To exemplify the impact of different types of jacket on the seismic vulnerability of the scoured bridge, fragility curves were generated with some typical values of jacket thickness selected from their studied range (i.e., 0–25.4 mm for steel jacket and 0–2.54 mm for composite jackets). Figure 5.5 shows fragility curves of the bridge at minor, moderate, and major damage states for four different retrofit cases in the presence of 2.4 m scour at bridge foundations: (a) with no retrofit (0 jacket thickness), (b) with 12.7-mm-thick steel jacket, (c) with 2.54-mm-thick carbon fiber composite jacket, and (d) with 2.54-mm-thick glass fiber composite jacket. As can be seen from this figure, considerable enhancements in the seismic fragility characteristics of the scoured bridge were obtained due to the application of jackets around bridge columns. For the same thickness of carbon fiber and glass fiber composite jackets, the carbon fiber composite jacket showed more effectiveness in improving the seismic vulnerability of the bridge. In comparison with 5-times-thicker steel jacket, the carbon fiber composite jacket was still effective in enhancing seismic fragility characteristics of the bridge in the presence of scour. Developed fragility curves of the bridge for different retrofit options were used further to obtain bridge failure probabilities for the evaluation of resilience under the same multi-hazard condition.

Figure 5.6 shows loss ratios and resilience of the bridge for some typical retrofit cases (cases considered to show the fragility curves in Figure 5.5). With all combinations of design variables of

bridge retrofit considered for this study, the maximum resilience of the bridge was obtained to be equal to 72%.

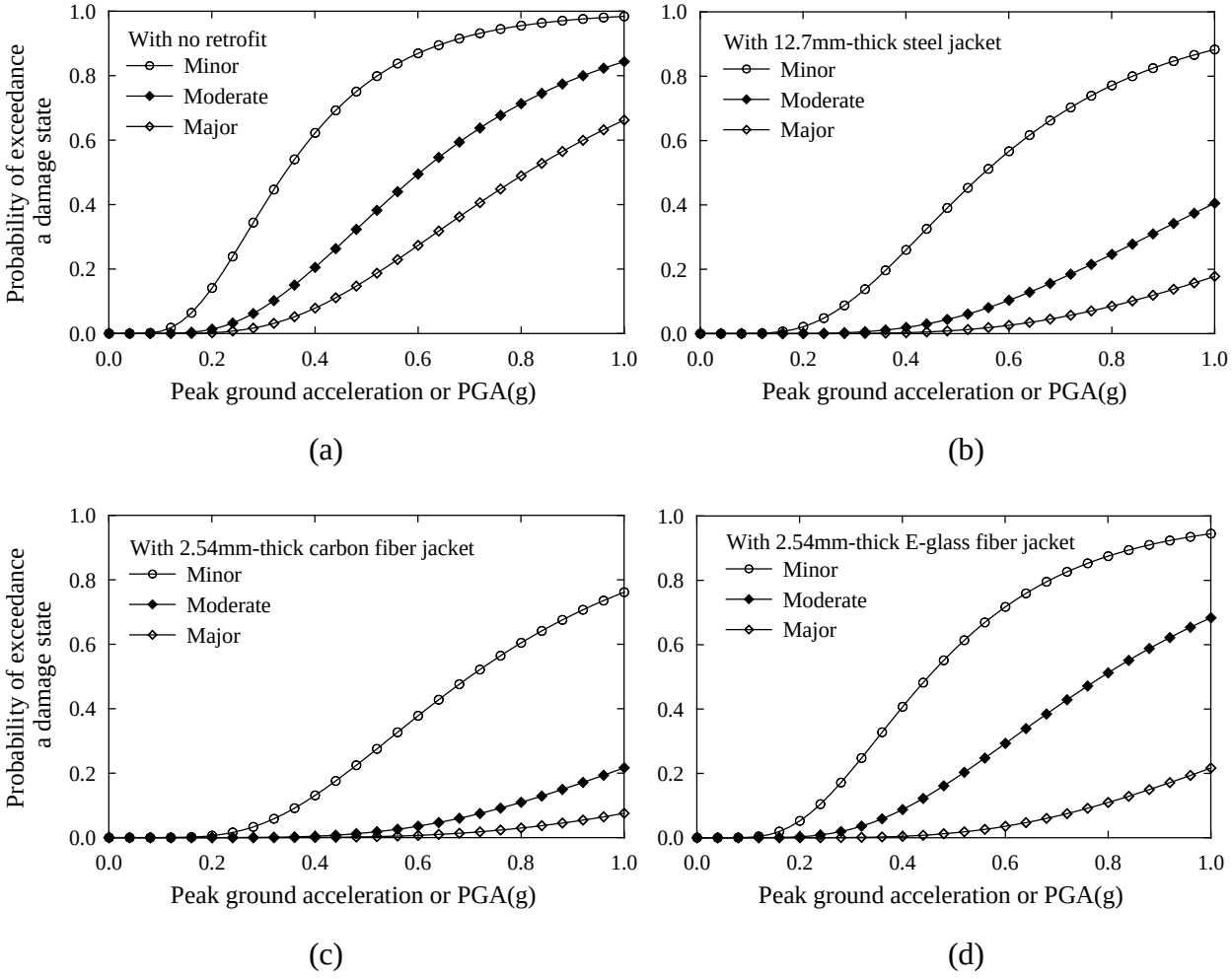

Figure 5.5: Fragility curves of the bridge with 2.4 m scour: (a) the original bridge with no retrofit, (b) retrofitted bridge with 12.7-mm-thick steel jacket, (c) retrofitted bridge with 2.54-mm-thick carbon fiber jacket, and (d) retrofitted bridge with 2.54-mm-thick E-glass fiber jacket

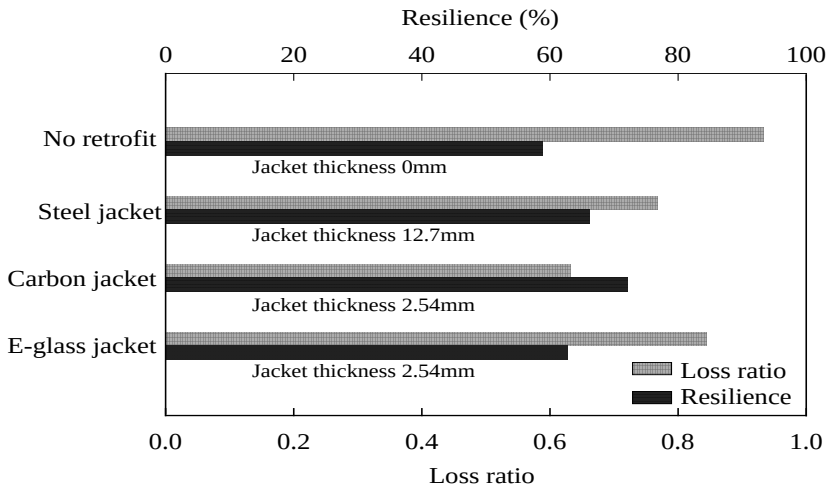

Figure 5.6: Resilience and loss ratios of the case study bridge for four retrofit cases

5.5. Optimal Retrofit Solution

Figures 5.7(a), (b), and (c) show the Pareto fronts obtained after the first three generations. The structural definitions of ten Pareto-optimal design solutions are listed in Tables 5.3, 5.4, and 5.5 respectively for generations 1, 2, and 3. As can be seen, the algorithm yielded the maximum resilience value of 70.5% at the end of all three generations.

From separate analyses with all possible retrofit design options, a maximum resilience value of 72% was obtained when all bridge columns were retrofitted with a 2.54-mm-thick carbon fiber composite jacket. However, the algorithm presented 70.5% as maximum resilience because of a variety of jacket thickness selected for different columns of the bridge. This is also evident from Tables 5.2 (a), (b), and (c). As these tables show, none of the optimal solutions used the same jacket thickness for all four bridge columns. In some cases, zero jacket thickness was selected for one of four bridge columns. This implies that the algorithm did not choose any retrofit for that column for obtaining an optimal solution. From generation 3, #1-8 provide the design solution with maximum resilience (i.e., minimum 'negative resilience', O_1) and #10 is the design solution with minimum cost of retrofit (i.e., O_2). Each of these solutions is equally important, as a particular retrofit design strategy can be selected from these solutions based on the preference. In case the resilience objective is given higher preference for the case

study bridge, design solution #5 (corresponding to minimum cost amongst #1-8) should be considered. On contrary, if the cost of retrofit were to be the restriction, #10 would be the most optimal retrofit solution for the case study bridge.

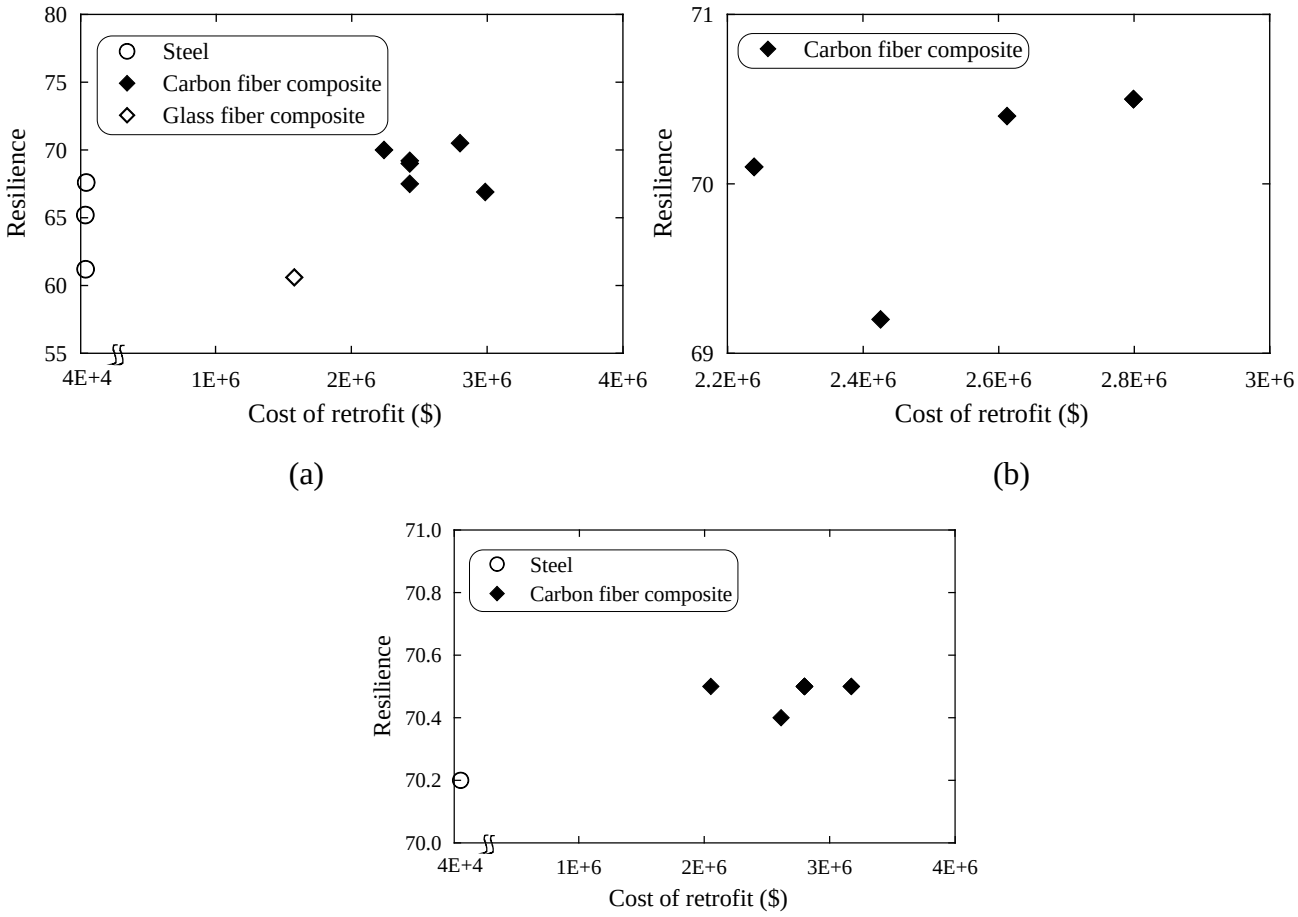

Figure 5.7: Pareto fronts from (a) generation 1, (2) generation 2, and (c) generation 3

Table 5.2(a) Retrofit design solutions from generation 1

Solution #	Material #	Thickness of jacket (mm)				Cost ($)	Resilience (%)
		Column 1	Column 2	Column 3	Column 4		
1	2	1.5	2.0	2.0	1.0	2.43E+06	69.0
2	2	1.5	2.0	2.0	1.0	2.24E+06	70.0
3	2	1.5	1.5	2.5	1.0	2.43E+06	69.2
4	1	2.5	25.4	15.2	15.2	4.85E+04	67.6
5	2	1.5	1.5	1.5	2.0	2.43E+06	67.5
6	2	2.5	0.5	2.5	2.5	2.99E+06	66.9
7	1	10.2	10.2	10.2	20.3	4.22E+04	65.2
8	2	2.0	2.5	2.5	0.5	2.80E+06	70.5
9	1	20.3	2.5	15.2	15.2	4.41E+04	61.2
10	3	1.5	1.0	2.0	2.0	1.58E+06	60.6

Table 5.2(b) Retrofit design solutions from generation 2

Solution #	Material #	Thickness of jacket (mm)				Cost ($)	Resilience (%)
		Column 1	Column 2	Column 3	Column 4		
1	2	2.0	2.5	2.5	0.5	2.80E+06	70.5
2	2	2.5	2.5	1.5	1.0	2.80E+06	70.5
3	2	2.0	2.5	2.5	0.5	2.80E+06	70.5
4	2	2.0	2.5	2.5	1.5	2.80E+06	70.5
5	2	0.0	2.5	2.0	1.0	2.80E+06	70.5
6	2	2.0	2.5	2.0	0.5	2.61E+06	70.4
7	2	1.0	2.0	2.0	1.0	2.24E+06	70.1
8	2	1.0	2.0	2.0	1.0	2.24E+06	70.1
9	2	1.5	1.5	2.5	1.0	2.43E+06	69.2
10	2	1.5	1.5	2.5	1.0	2.43E+06	69.2

Table 5.2(c) Retrofit design solutions from generation 3

Solution #	Material #	Thickness of jacket (mm)				Cost ($)	Resilience (%)
		Column 1	Column 2	Column 3	Column 4		
1	2	2.0	2.5	2.5	0.5	2.80E+06	70.5
2	2	2.5	2.5	1.5	1.0	2.80E+06	70.5
3	2	2.0	2.5	2.5	0.5	2.80E+06	70.5
4	2	2.0	2.5	2.5	1.5	3.17E+06	70.5
5	2	0.0	2.5	2.0	1.0	2.05E+06	70.5
6	2	2.0	2.5	2.5	1.5	3.17E+06	70.5
7	2	2.5	2.5	1.5	1.0	2.80E+06	70.5
8	2	2.0	2.5	2.5	0.5	2.80E+06	70.5
9	2	2.0	2.5	2.0	0.5	2.61E+06	70.4
10	1	15.2	25.4	25.4	5.1	5.91E+04	70.2

6. CONCLUSIONS

The seismic resilience of a multi-span reinforced concrete highway bridge was first estimated in the present study. The bridge experienced severe damage during the 1994 Northridge earthquake due to shear failure of one bridge pier in the transverse direction of the bridge. The present study developed the seismic vulnerability model of the bridge in the form of fragility curves at different bridge damage states. These curves provide 100%, 99.7%, 95.3%, and 93.5% failure probabilities of the bridge, respectively, in the minor, moderate, major damage, and complete collapse states due to lateral shaking induced by the horizontal ground motion component of the Northridge earthquake. These failure probability values also predict bridge damage at higher damage states under the Northridge earthquake. From these failure probabilities, direct and indirect losses due to bridge damage were calculated. Seismic resilience of the bridge was evaluated by combining seismic vulnerably and loss models with a suitable post-earthquake recovery model considered for the bridge. The study explored three different recovery models and observed that the linear recovery model, which resulted in 57.47% seismic resilience of the bridge, is the most suitable model for the current purpose.

The latter part of the study presented an optimal retrofit design method for highway bridges by making use of a multi-objective evolutionary algorithm, namely Non-Dominated Sorting Genetic Algorithm II (NSGA II). The impact of various bridge retrofit design options (i.e., column jacketing with steel composite casings) was studied under the multi-hazard effect of earthquake and flood-induced scour. It was considered that the bridges were pre-exposed to flood hazards that resulted in bridge scour before the occurrence of seismic events. The optimization algorithm evaluated the disaster resilience of the bridge under the multi-hazard condition by applying all possible retrofit options generated based on the user-specified bounds on design variables. In addition, it calculated the cost for each of these retrofit options. The algorithm yields optimal retrofit design solutions through the minimization of negative

resilience (i.e., maximization of resilience) and cost of retrofit. Demonstration of this optimization problem through a case study bridge under the stated multi-hazard condition provided optimal retrofit design solutions that pertain to the bridge and retrofit configurations selected for this case study. This optimal set of solutions offered the best search results for retrofit material and configuration. Hence, obtained optimal solutions facilitated the choice of a retrofit strategy based on specific preferences on target resilience and retrofit cost.

REFERENCES

Abrahamson, N., Silva, W. (2008). "Summary of the Abrahamson & Silva NGA ground motion relations." *Earthquake Spectra*, 24 (1), 67-97.

Alampalli, S., and Ettouney, M. (2008). "Multihazard applications in bridge management," *Transportation Research Circular*, Number E-C128, Transportation Research Board.

Amdal, J. R., and Swigart, S. L. (2010). "Resilient transportation systems in a post-disaster environment: a case study of opportunities realized and missed in the greater New Orleans region." UNOTI Publications: Paper 5.

Ang, A., and Tang, W. (1984). *Probability Concepts in Engineering Planning and Design: Decision, Risk, and Reliability*. John Wiley & Sons, New York.

Applied Technology Council (1985). "Earthquake Damage Evaluation Data for California." Applied Technology Council, ATC-13, Redwood City, CA.

Arcidiacono, V., Cimellaro, G. P., Reinhorn, A. M., and Bruneau, M. (2012). "Community resilience evaluation including interdependencies." 15th World Conference on Earthquake Engineering (15WCEE), Lisbon, Portugal.

Banerjee, S., and Prasad, G. G. (2013). "Seismic Risk Assessment of Reinforced Concrete Bridges in Flood-Prone Regions." *Structure and Infrastructure Engineering*, 9(9), 952-968.

Banerjee, S., and Shinozuka, M. (2008a). "Mechanistic Quantification of RC Bridge Damage States under Earthquake through Fragility Analysis." *Probabilistic Engineering Mechanics*, 23(1), 12-22.

Banerjee, S., and Shinozuka, M. (2008b). "Experimental Verification of Bridge Seismic Damage States Quantified by Calibrating Analytical Models with Empirical Field Data." *Journal of Earthquake Engineering and Engineering Vibration*, 7(4), 383-393.

Bocchini, P., and Frangopol, D. (2012). “Optimal Resilience- and Cost-Based Postdisaster Intervention Prioritization for Bridges along a Highway Segment.” *J. Bridge Eng.*, 17(1), 117–129.

Broderick, B. M., and Elnashai, A. S. (1994). “Analysis of the failure of Interstate 10 Freeway ramp during the Northridge earthquake of 17 January 1994.” *Earthquake Engineering and Structural Dynamics*, 24: 189-208.

Bruneau, M., Chang, S., Eguchi, R., Lee, G., O’Rourke, T., Reinhorn, A., Shinozuka, M., Tierney, K., Wallace, W., and von Winterfelt, D. (2003). “A framework to quantitatively assess and enhance the seismic resilience of communities.” *Earthquake Spectra*, 19 (4): 733-752.

Caltrans (1997). Contact Cost Data. http://sv08data.dot.ca.gov/contractcost/index.php

Caltrans (2011a). “Seismic Retrofit Program.” http://www.dot.ca.gov/hq/paffairs/about/retrofit.htm (February 14, 2011).

Caltrans (2011b). “Bridge Standard Detail Sheets.” State of California Department of Transportation Division of Engineering Services.
www.dot.ca.gov/hq/esc/techpubs/manual/bridgemanuals/bridge-standard-detail-sheets/pdf/sec7/xs7-020.pdf

Caltrans (2011c). “Bridge Standard Detail Sheets.” State of California Department of Transportation Division of Engineering Services.
www.dot.ca.gov/hq/esc/techpubs/manual/bridgemanuals/bridge-standard-detail-sheets/pdf/sec7/xs7-020.pdf xs7-020.pdf

Chang, S., and Chamberlin, C. (2004). “Assessing the role of lifeline systems and community disaster resilience.” *MCEER Research Progress and Accomplishments*, Buffalo, NY.

Chang, S. E., and Nojima, N. (2001). "Measuring post-disaster transportation system performance: the 1995 Kobe earthquake in comparative perspective." *Transportation Research Part A: Policy and Practice*, 35 (6): 475-494.

Chang, E. S., Shinozuka, M., and Moore, J. (2000). 'Probabilistic earthquake scenarios: extending risk analysis methodologies to spatially distributed systems.' *Earthquake Spectra*, 16 (3), 557 - 572.

Cimellaro, G. P., Reinhorn, A. M., and Bruneau, M. (2010). "Framework for analytical quantification of disaster resilience." *Engineering Structures*, 32: 3639-3649.

Cimellaro G. P. (2013). "Resilience-based design (RBD) modelling of civil infrastructure to assess seismic hazards." *Handbook of Seismic Risk Analysis and Management of Civil Infrastructure Systems*, Edited by S. Tesfamariam, Canada and K. Goda, University of Bristol, UK, Woodhead Publishing Limited.

Cofer, W. F., Mclean, D. I., and Zhang, Y. (1997). *Analytical Evaluation of Retrofit Strategies for Multi-Column Bridges*. Technical Report for Washington State Transportation Centre (TRAC); Washington State University, Pullman, Washington.

Cutter, S. L., Ahearn, J. A., Amadei, B., Crawford, P., Eide, E. A., Galloway, G. E., and Zoback, M. L. (2013). "Disaster Resilience: A National Imperative." *Environment: Science and Policy for Sustainable Development*, 55(2), 25-29.

Deb, K. (2001). *Multi-objective Optimization using Evolutionary Algorithms*, John Wiley & Sons, Ltd, West Sussex, England.

Deb, K., Pratap, A., Agarwal, S., and Meyarivan, T. (2002). "A Fast and Elitist Multiobjective Genetic Algorithm: NSGA-II," *Evolutionary Computation, IEEE Transactions*, 6(2), 182–197.

Dennemann, L. K. (2009). "Life-Cycle Cost Benefit (LCC-B) Analysis for Bridge Seismic Retrofits." MS Thesis, Rice University, TX.

Fallah, N., and Zamiri, G. (2012). “Multi-objective optimal design of sliding base isolation using genetic algorithm.” *Scientia Iranica, Transactions A: Civil Engineering*, DOI: 10.1016/j.scient.2012.11.004.

FEMA (2008). *Flood Insurance Study for Sutter County, California*, Federal Emergency Management Agency (FEMA) Flood Insurance Study Number 060394V000A.

FHWA. (2006). *Seismic Retrofitting Manual for Highway Structures: Part 1 – Bridges, Federal Highway Management Agency*. Publication No. FHWA-HRT-06-032.

Ghosn, M., Moses, F., and Wang, J. (2003). *Highway Bridge Design for Extreme Events*. National Cooperative Highway Research Program, NCHRP Report 489, Transportation Research Board, National Academy Press, Washington DC.

Haroun, M. and Elsanadedy, H. (2005). “Fiber-Reinforced Plastic Jackets for Ductility Enhancement of Reinforced Concrete Bridge Columns with Poor Lap-Splice Detailing.” *J. Bridge Eng*., 10(6), 749–757.

HAZUS. (1999). *Earthquake Loss Estimation Methodology*. Technical Manual SR2, Federal Emergency Management Agency, through agreements with National Institute of Building Science, Washington, D.C.

HAZUS–MH MR3. (2003). *Multi-hazard Loss Estimation Methodology – Earthquake Model*. Technical Manual, Department of Homeland Security, Washington, D.C.

Lee, D. H., and Elnashai, A. S. (2002). “Inelastic seismic analysis of RC bridge piers including flexure-shear interaction.” *Structural Engineering and Mechanics*; 12 (3): 241-260.

Computer and Structures, Inc. (2011). SAP2000 (Structural Analysis Program), Berkeley, CA, Version 15.0.

MCEER-AEI (2007). “Symposium on Emerging Developments in Multi-hazard Engineering.” McGraw-Hill Auditorium, New York City. <http://mceer.buffalo.edu/meetings/AEI/steering.asp>.

McKay, M. D. (1992). “Latin hypercube sampling as a tool in uncertainty analysis of computer models.” Proceedings of the 24th Winter Simulation Conference, Virginia, 1992; 557 - 564.

McKenna, F., and Fenves, G. L. (2012). “Open System for Earthquake Engineering Simulation, Version 2.4.0.” Pacific Earthquake Engineering Research Center.

MTD 5-1. (1992). “Bridge Memo to Designers (5-1).” California Department of Transportation, Sacramento, CA.

Paton, D., and Johnston, D. (2006). “Disaster Resilience an Integrated Approach.” Charles C Thomas Publisher LTD., Cap. 4, Lifelines and Urban Resilience. ISBN 0-398-07663-4 – ISBN 0-398-07664-2.

Pekcan, G. (1998). “Design of Seismic Energy Dissipation Systems for Concrete and Steel Structures.” Ph.D. Dissertation, University at Buffalo, State University of New York, Buffalo, New York.

Prasad, G. G., and Banerjee, S. (2013). “The Impact of Flood-Induced Scour on Seismic Fragility Characteristics of Bridges.” *Journal of Earthquake Engineering*, 17(9), 803-828.

Priestley, M. J. N., Seible, F., and Calvi, G.M. (1996). *Seismic Design and Retrofit of Bridges*. John Wiley & Sons, Inc., New York, N.Y.

Richardson, E. V., and Davis, S. M. (2001). “Evaluating Scour at Bridges,” Publication No. FHWA NHI 01-001, Hydraulic Engineering Circular (HEC) No. – 18, Federal Highway Administration, U.S. Department of Transportation, Washington, D.C.

Rose, A., and Liao, S. E. (2005). “Modeling regional economic resiliency to earthquakes: a computable general equilibrium analysis of water service disruptions.” *Journal of Regional Science*, 45: 75-112.

Shinozuka, M., Chang, S. E., Cheng, T. C., Feng, M., O'Rourke, T. D., Saadeghvaziri, M. A., Dong, X., Jin, X., Wang, Y., and Shi, P. (2004). "Resilience of integrated power and water systems." *MCEER Research Progress and Accomplishments*, 65-86. Buffalo, NY.

Shinozuka, M., Feng, M.Q., Kim, H., Uzawa, T., and Ueda, T. (2000). *Statistical Analysis of Fragility Curves*. Technical Report, Multidisciplinary Center for Earthquake Engineering Research, State University at Buffalo, Buffalo, N.Y.

Sultan, M., and Kawashima, K. (1993). "Comparison of the seismic design of highway bridges in California and in Japan." Recent selected publications of Earthquake Engineering Div., Public Works Research Institute (PWRI), Japan (Technical Memorandum of PWRI No. 3276.

USGS. (2011). "National Water Information System." http://nwis.waterdata.usgs.gov/nwis, as visited on February 14, 2011.

Venkittaraman, A. (2013). "Seismic Resilience of Highway Bridges." MS Thesis, The Pennsylvania State University, University Park, PA.

Venkittaraman, A., and Banerjee, S. (2013). "Enhancing Resilience of Highway Bridges through Seismic Retrofit." *Earthquake Engineering and Structural Dynamics*, 43(8), 1173–1191.

Wright, T., DesRoches, R., and Padgett, J. E. (2011). "Bridge Seismic Retrofitting Practices in the Central and Southeastern United States." *Journal of Bridge Engineering*, 16(1), 82-92.

WSDOT. (2011). "Washington State's Bridge Seismic Retrofit Program." http://www.wsdot.wa.gov/eesc/bridge/preservation/pdf%5CBrgSeismicPaper.pdf (February 14, 2011).

Zhou, Y., Banerjee, S., and Shinozuka, M. (2010). "Socio-economic effect of seismic retrofit of bridges for highway transportation networks: A pilot study." *Structure and Infrastructure Engineering*, 6 (1–2), 145–157.